Development and application of tunable VUV laser sources

by
Anton Christiaan Nortje

Thesis presented in fulfillment of the requirements for the degree of Master of Science in the Faculty of Science at Stellenbosch University

Supervisor: Dr. Christine Steenkamp
Co-Supervisor: Prof. Erich Rohwer

March 2013

Stellenbosch University http://scholar.sun.ac.za

Declaration

By submitting this thesis/dissertation electronically, I declare that the entirety of the work contained therein is my own, original work, that I am the sole author thereof (save to the extent explicitly otherwise stated), that reproduction and publication thereof by Stellenbosch University will not infringe any third party rights and that I have not previously in its entirety or in part submitted it for obtaining any qualification.

March 2013

Copyright © 2013 Stellenbosch University

All rights reserved

Stellenbosch University http://scholar.sun.ac.za

Abstract

A tunable narrow-bandwidth vacuum ultra violet laser source was developed and characterised. Two-photon resonant four-wave sum-frequency mixing of two pulsed dye laser beams in magnesium vapour was used to generate the VUV laser light. A heat pipe oven with a concentric design was incorporated to provide a magnesium vapour column of around 30 cm in length with a sufficiently stable temperature and appropriate vapour pressure for efficient VUV production. This is a longer nonlinear medium length than previously produced in our laboratory using a crossed heat pipe oven. The longer medium facilitated the production of VUV laser light of higher intensity than was previously obtainable.

High resolution laser induced fluorescence spectra of carbon monoxide in a supersonic gas jet was recorded using the tunable VUV laser light produced in the crossed heat pipe oven. Experimental parameters were optimised and adjusted for the selective detection of the forbidden singlet-triplet transitions which typically have longer lifetimes than singlet-singlet transitions. Transitions from the $X^1\Sigma^+(v = 0)$ ground state to the $e^3\Sigma^-(v = 5)$ triplet state were recorded, and accurate wavelength for the spectral lines were determined. Laboratory wavelengths for these lines have not been measured previously. Accurate wavelength for the weak forbidden spectral lines of CO are important in astrophysical applications, for example determining column densities of interstellar gas clouds.

Stellenbosch University http://scholar.sun.ac.za

Opsomming

'n Afstembare smal bandwydte vakuum ultraviolet laser bron is ontwikkel en gekarakteriseer. Twee-foton resonante vier-golf som-frekwensie vermenging van twee gepulseerde kleurstoflaserbundels in 'n magnesium damp is gebruik om die VUV laser lig te produseer. 'n Hittepyp oond met 'n konsentriese ontwerp is in gebruik geneem om a magnesium damp kollom van ongeveer 30 cm in lengte te voorsien waarvan die temperatuur voldoende stabiel is en die dampdruk toepaslik is vir effektiewe VUV produksie. Dit is 'n langer nie-liniêre medium as wat in die verlede deur 'n kruis-hittepyp oond voorsien is. Die langer medium het dit moontlik gemaak om VUV laser lig van hoër intensiteit te produseer as wat tot dusver bereikbaar was.

Hoë resolusie laser geinduseerde fluoresensie spektra van koolstof monoksied in a supersoniese gasstraal is opgeneem met die hulp van die afstembare VUV laser lig geproduseer in die kruis-hittepyp oond. Eksperimentele parameters is geoptimeer en verstel vir die selektiewe waarneming van die verbode singlet-triplet oorgange wat tipies langer leeftye besit in vergelyking met singlet-singlet oorgange. Oorgange vanaf die $X^1\Sigma^+(v = 0)$ grond toestand na die $e^3\Sigma^-(v = 5)$ triplet toestand is opgeneem en akkurate golflengtes vir die spektrale lyne is bepaal. Laboratorium golflengtes het tot dusver nie bestaan vir hierdie lyne nie. Akkurate golflengtes vir die swak verbode spektrale lyne van CO het belangrike toepassings in astrofisika soos die bepaling van die kollom digtheid van interstellêre gas wolke.

Stellenbosch University http://scholar.sun.ac.za

Acknowledgments

First and foremost I would like to thank my promoters for my M.Sc. study, Christine Steenkamp and Erich Rohwer for supporting me throughout, and for always being available to help. This thesis would never have seen the light of day without them.

Many thanks to Ulli Deutschländer for technical support and advise. Also thanks to Johan Germishuizen for support with equipment in the laboratory. I would like to thank Eben Shields from the electronics workshop for help with electronic equipment, especially the PMT circuit boards.

Thanks to the staff of the mechanical workshop, Boel Botha, John Burns and Dawid Pool, for manufacturing various items of equipment for the laboratory in aid of my studies.

I am very grateful for all the staff and students at the physics department who provided support to me during my studies. I specifically extend my thanks to the members of the LRI who welcomed me at the institute and went out of their way to help wherever they could.

Also thanks to all family and friends for their support during my studies.

Stellenbosch University http://scholar.sun.ac.za

Contents

Stellenbosch University http://scholar.sun.ac.za

Stellenbosch University http://scholar.sun.ac.za

List of Figures

Stellenbosch University http://scholar.sun.ac.za

Stellenbosch University http://scholar.sun.ac.za

List of Tables

Stellenbosch University http://scholar.sun.ac.za

Chapter 1

Problem statement

1.1 Motivation

A tunable narrow bandwidth laser source in the VUV region of the spectrum can be applied to the spectroscopy of small molecules that do not absorb light at lower frequencies. For larger molecules it can be used for one-photon ionisation in time of flight studies using a mass spectrometer.

Laboratory study of the spectrum of carbon monoxide (CO) has important applications in astronomy. CO spectra in the radio frequency, infrared and vacuum ultraviolet (VUV) range of the spectrum are recorded by satellite based spectrographs. The absorption lines of CO in these observations yield data on the composition of interstellar gas clouds and the evolution of stars. [4][5]

The column densities of CO in interstellar space is determined most accurately from weak absorption lines in the VUV range, like the ones arising from forbidden singlet-triplet transitions. For many of these lines accurate laboratory wavelengths have not been measured. This study will therefore contribute to the recording of these forbidden spectral lines that occur in the VUV region of the spectrum.

No commercial narrow bandwidth, wavelength tunable, coherent VUV sources exist. Such a source can be obtained by the conversion of visible laser beams into a VUV beam by means of sum frequency generation in a nonlinear optical medium. Suitable nonlinear crystals for generation of VUV light do not exist as the available nonlinear crystals strongly absorb that range of wavelengths. Metal vapours can be utilised as nonlinear media because they posses sufficiently high third order nonlinear susceptibilities. Metal vapours are centrosymmetric, meaning second order nonlinear processes are forbidden and third order processes must be used. In order to produce a magnesium vapour with high enough vapour pressure a stable temperature of around 750 °C is required. This stable high temperature environment can be produced inside a heat pipe oven.

In our laboratory a tunable VUV laser source has been produced previously using a crossed heat pipe oven [6]. This source has been successfully applied to the spectroscopic study of CO. In this study we characterise a new concentric heat pipe oven that will be employed for spectroscopic studies in future. The concentric heat pipe will provide a longer nonlinear medium which is expected

Stellenbosch University http://scholar.sun.ac.za

to yield higher intensity VUV laser light. The higher intensity obtained will aid the detection of weak forbidden transitions of CO.

1.2 Aim

The aim of this thesis is the implementation of a concentric heat pipe oven to generate a magnesium vapour nonlinear medium for VUV generation by sum frequency generation. The VUV source, using the concentric heat pipe, will be characterised and compared to the crossed heat pipe as applied in previous studies.

An investigation will be made into the effect of the longer nonlinear medium produced by the concentric heat pipe on phase matching and VUV production.

The effect of focusing conditions of the incoming laser beam on the phase matching curves and the intensity of VUV production will be investigated. In particular we will investigate the effect on the modulation depth in the phase matching curve for focusing in the regime between the tightly focused limit and the parallel beam limit as this is not described analytically in theory.

We will investigate how experimental conditions can be optimized for the application of spectroscopy of CO and look at how various experimental variables can be adjusted to aid the observation of singlet-triplet transitions in CO.

Stellenbosch University http://scholar.sun.ac.za

Chapter 2

Literature Review

2.1 A tunable VUV laser source

Tunable narrow bandwidth VUV for spectroscopy is generated in our VUV source by the four-wave sum frequency process. The tunable VUV frequency is given by $\omega_{vuv} = 2\omega_1 + \omega_2$ Where ω_1 is the frequency of a dye laser tuned to a two-photon resonance of magnesium, and ω_2 is the tunable frequency of a second dye laser. However for characterisation of the VUV source third harmonic generation of the resonant dye laser is generally used to produce the VUV frequency $\omega_3 = 3\omega_1$.

2.1.1 Third harmonic generation

Narrow bandwidth VUV laser light can be produced via third harmonic generation in a medium with a sufficiently large third order nonlinear susceptibility. The starting point is the fundamental equation of nonlinear optics [7]

$$\nabla \times \nabla \times \tilde{E}_n(r) + \frac{\epsilon^{(1)}(\omega_n)}{c^2}.\frac{\partial^2 \tilde{E}_n(r)}{\partial t^2} = -\frac{4\pi}{c^2}\frac{\partial^2}{\partial t^2}\tilde{P}_n^{NL}(r) \tag{2.1}$$

where $\tilde{E}_n(r)$ is the electric field, $\tilde{P_n^{NL}}(r)$ is the nonlinear component of the polarisation, $\epsilon^{(1)}(\omega_n)$ is the real, frequency-dependent dielectric tensor, and c is the speed of light in vacuum.

An equation describing third harmonic generation is derived from 2.1 by making the following assumptions:

- We assume that the electric fields of the incident wave as well as the generated wave can be described as plane waves propagating in the z-direction. This corresponds to the parallel beam limit, assuming collimated laser beams.
- The intensity of the fundamental laser beam is not attenuated by the nonlinear optical process but only by one-photon absorption. This is called the small signal limit.

Stellenbosch University http://scholar.sun.ac.za

- The fraction by which the amplitude of the electric field A_3 changes over the distance of an optical wavelength is much smaller than 1. This is known as the slow varying amplitude approximation.
- The nonlinear medium is approximated to be rectangular.

The third harmonic intensity will then be given by

$$I_3(L) = \frac{144\pi^4\omega_3^2}{c^4 n_1^3 n} L^2 \left[\chi^{(3)}\right]^2 I_1^3(0) F(\Delta k,\, L) \tag{2.2}$$

where the phase matching factor is given by

$$F(\Delta kL,\, \Gamma_i,\, \Gamma_s) = \frac{exp(-\Gamma_i) + exp(-\Gamma_s) - 2exp\left(-\frac{\Gamma_i+\Gamma_s}{2}\right) cos(\Delta kL)}{\left(\frac{\Gamma_s-\Gamma_i}{2}\right)^2 + (\Delta kL)^2} \tag{2.3}$$

Where L is the length of the nonlinear medium. The wave vector mismatch Δk, and the optical depths for the incoming and third harmonic beams, Γ_i and Γ_s, are defined as:

$$\triangle k = 3k_1 - k_3 \tag{2.4}$$

$$\Gamma_s = \sigma_3 NL$$

$$\Gamma_i = 3\sigma_1 NL$$

where σ is the absorption cross section and N the number density of the medium. The complete derivation of equation 2.1 can be seen elsewhere [6].

The third harmonic intensity I_3 is optimised by:

- A two-photon resonance with the energy levels of the nonlinear medium. This optimises the value of $\chi^{(3)}$ [7].
- High incident intensity $I_1(0)$.
- A long nonlinear medium length L.
- Phase matching of the medium, which optimises the value of $F(\Delta k, L)$.

For sum frequency generation it is important to suppress third harmonic generation, as it is a competing process that will reduce the intensity of the light obtained from the sum frequency process. This can be done by circularly polarising the dye laser beams of the respective dye lasers with opposite directions of circular polarisation.

Stellenbosch University http://scholar.sun.ac.za

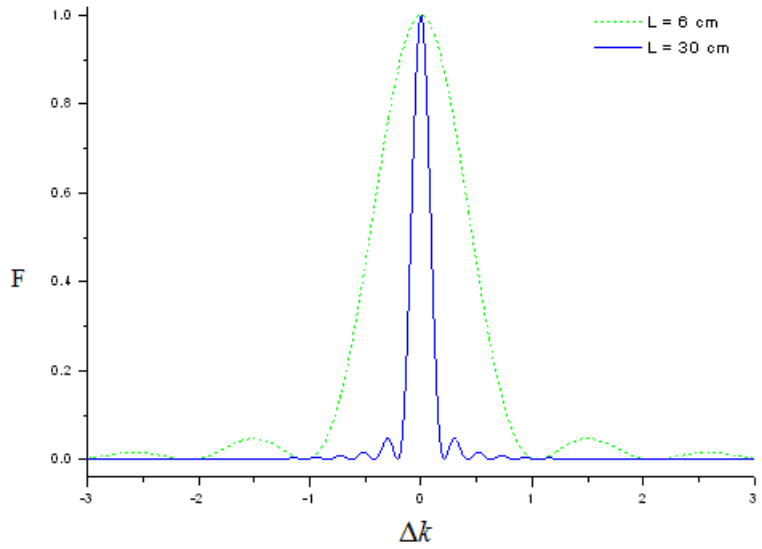

Figure 2.1: The phase matching factor F as a function of the wave vector mismatch plotted for different lengths of nonlinear medium.

2.1.2 Phase matching for parallel beams

Phase matching corresponds to the requirement for the conservation of linear momentum during the third harmonic generation process. The wave vector $k = \frac{p}{\hbar}$ relates to the linear momentum of the wave. The wave vector mismatch, Δk, defined in equation 2.4, gives an indication of the conservation of momentum, where $\Delta k = 0$ corresponds to perfect phase matching. For third harmonic generation $\Delta k = 0$ is equivalent to the refractive indices inside the medium being equal for the incident and third harmonic beams, i.e. $n_3 = n_1$. Magnesium shows anomalous dispersion within the frequency range of the incident beam, so $n(\omega_1)_{Mg} > n(\omega_3)_{Mg}$. Krypton shows normal dispersion in the same frequency region, giving $n(\omega_1)_{Kr} < n(\omega_3)_{Kr}$. If magnesium vapour and Krypton gas is mixed in the correct ratio the refractive indices will therefor be the same for the incident and the third harmonic beams and in this way the phase matching requirement can be satisfied.

The general equation for the phase matching factor, equation 2.3, can be simplified for the case of an optically thin medium where Γ_s and Γ_i goes to zero

$$F(\Delta kL, \Gamma_i \to 0, \Gamma_s \to 0) \approx \left(\frac{sin(\Delta kL/2)}{\Delta kL/2} \right)^2 \tag{2.5}$$

This has been plotted in figure 2.1 for two different values of L.

In practice the nonlinear medium and fundamental frequency can be chosen in such a way that the fundamental frequency does not correspond to electric dipole transitions of the medium. This will minimise Γ_i making the approximation $\Gamma_i \to 0$ fairly accurate. The third harmonic frequency however is often

Stellenbosch University http://scholar.sun.ac.za

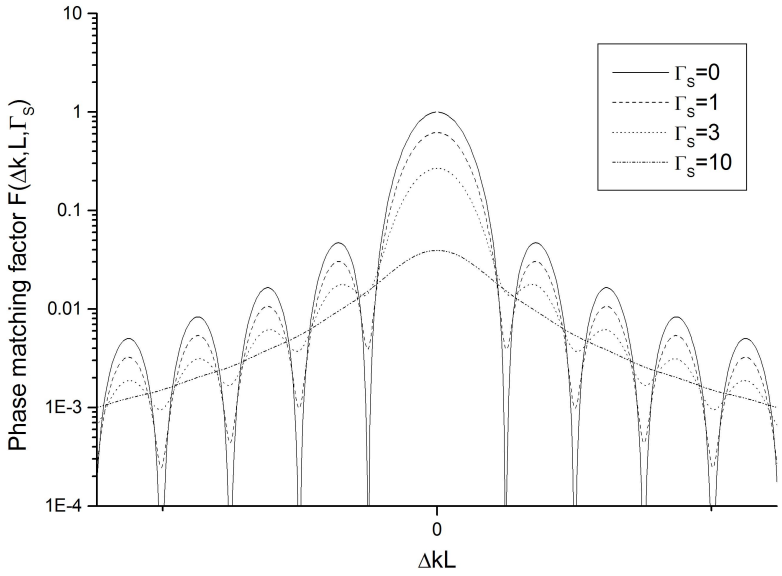

Figure 2.2: The phase matching factor as function of the wave vector mismatch for different values of optical depth, plotted with a logarithmic scale on the y-axis.

associated with auto-ionisation or photo-ionisation of the medium that cannot be minimised and has to be taken into account [8]. This makes the phase matching factor dependent on the optical depth of the medium. Starting again from the general expression for the phase matching factor, equation 2.3, and approximating the optical depth for the incoming frequencies $\Gamma_i = 0$, the phase matching factor becomes

$$F(\Delta kL,\, \Gamma_s) = \frac{1 + exp(-\Gamma_s) - 2exp\left(-\frac{\Gamma_s}{2}\right) cos(\Delta kL)}{\left(\frac{\Gamma_s}{2}\right)^2 + (\Delta kL)^2} \tag{2.6}$$

By plotting this equation for various values of optical depth as shown in figure 2.2 we notice a decrease in the modulation depth of the curve as the optical depth increases. The maxima of the modulation occur when $cos(\Delta kL) = -1$. Substituting this into equation 2.6 we get a curve bounding the peaks of the phase matching factor curve

$$F(\Delta kL,\, \Gamma_s)_{max} = \frac{1 + exp(-\Gamma_s) + 2exp\left(-\frac{\Gamma_s}{2}\right)}{\left(\frac{\Gamma_s}{2}\right)^2 + (\Delta kL)^2} \tag{2.7}$$

The same can be done for the minima occurring at $cos(\Delta kL) = 1$, giving a curve bounding the minima of the phase matching factor curve

$$F(\Delta kL,\, \Gamma_s)_{min} = \frac{1 + exp(-\Gamma_s) - 2exp\left(-\frac{\Gamma_s}{2}\right)}{\left(\frac{\Gamma_s}{2}\right)^2 + (\Delta kL)^2} \tag{2.8}$$

The phase matching factor together with the two bounding curves are plotted

Stellenbosch University http://scholar.sun.ac.za

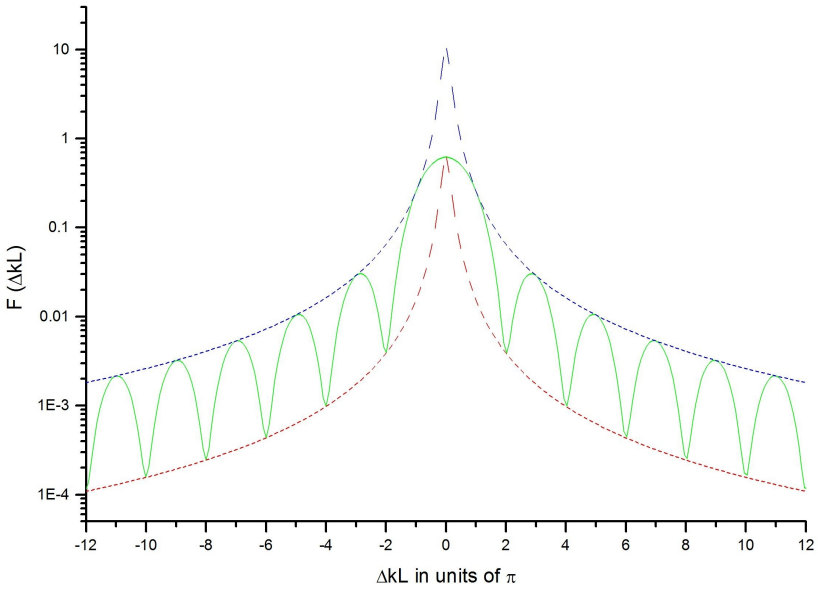

Figure 2.3: The phase matching factor F for $\Gamma_s = 1$ with the maximum and minimum curves shown as dashed lines.

in figure 2.3 for an optical depth Γ_s =1. The modulation depth M can be calculated by taking the ratio of equation 2.7 to equation 2.8

$$M = \frac{1 + exp(-\Gamma_s) + 2exp\left(-\frac{\Gamma_s}{2}\right)}{1 + exp(-\Gamma_s) - 2exp\left(-\frac{\Gamma_s}{2}\right)} \tag{2.9}$$

Substituting $z = exp\left(-\frac{\Gamma_s}{2}\right)$ this becomes

$$M = \frac{1 + 2z + z^2}{1 - 2z + z^2} \tag{2.10}$$

this can be solved for z giving

$$z = \frac{2(M+1) \pm \sqrt{4(M+1)^2 - 4(M-1)^2}}{2(M-1)} \tag{2.11}$$

where the optical depth in terms of z is given by

$$\Gamma_s = -2\, ln\, z \tag{2.12}$$

This provides us with a way to relate the modulation depth observed in a phase matching curve to the optical depth of the nonlinear medium.

2.1.3 Phase matching for focused beams

In practice the incoming laser beam is often focused inside the medium in order to increase the efficiency of the nonlinear process by increasing the intensity of

Stellenbosch University http://scholar.sun.ac.za

the beam inside the medium. In such a case the parallel beam approximation is no longer valid. To determine the effect of focusing on phase matching we have to consider an incoming beam with a Gaussian intensity distribution [9]

$$E_q(r,\, z,\, t) = E_q(r,\, z)\frac{b}{b+2iz} exp\left(\frac{-k_q r^2}{b+2iz}\right) exp(ik_q z) \tag{2.13}$$

where the confocal parameter b is

$$b = 2z_0 = \frac{2\pi\omega_0^2}{\lambda} = k\omega_0^2 \tag{2.14}$$

with ω_0 the $1/e^2$ radius of the intensity distribution in the focal plane, and z_0 the Rayleigh length.

By making the approximations that absorption can be neglected and that the medium is close to phase matching, the phase matching factor can be shown to be [9, 8]

$$F(\Delta k,\, L,\, b) = \frac{1}{L^2}\left[\int_{\frac{-L}{2}}^{\frac{+L}{2}} \frac{exp(-i\Delta kz)}{(1+\frac{2iz}{b})^2}\, dz\right] \tag{2.15}$$

In the case of tight focusing only the section of the medium in the beam waist of length b contribute to the nonlinear process making the length of the medium unimportant. The integral limits can therefor be extended to infinity and the equation can be solved analytically resulting in [9, 8]

$$F(\Delta kb,\, b/L \ll 1) = 0 \quad \text{for} \quad \Delta kb \geq 0$$

and

$$F(\Delta kb,\, b/L \ll 1) = \frac{\pi^2}{4}\left(\frac{b}{L}\right)^2 (\Delta kb)^2 exp(\Delta kb) \tag{2.16}$$

$$\text{for} \quad \Delta kb < 0$$

This function has a maximum of $\left(\frac{\pi b}{eL}\right)^2$ at $\Delta kb = -2$. Hence the maximum of the phase matching curve shifts towards negative Δk values when tight focusing is applied to the incoming beam. This can be seen in a plot of the equation in figure 2.4. When Δk has a small negative value we have $|k_{3\omega}| < 3|k_\omega|$. Under these conditions some of the nonparallel components of the focused beam can satisfy the phase matching condition and contribute to VUV production in the medium.

2.1.4 The heat pipe oven as spectroscopic device

The crossed and concentric heat pipe ovens used in this study for VUV generation was developed by Scheingraber and Vidal [10][11]. A brief overview of the operating principles of a heat pipe oven will be given here. For a more comprehensive description see chapter 4 of reference [6]. This discussion will refer to the crossed heat pipe oven and specific working materials as used in our setup.

The crossed heat pipe oven, shown in figure 2.5, comprises two heat pipes - A vertical pipe with sodium as working material filled with argon gas at pressure P_1, and a horizontal pipe of smaller diameter passing through the vertical pipe

Stellenbosch University http://scholar.sun.ac.za

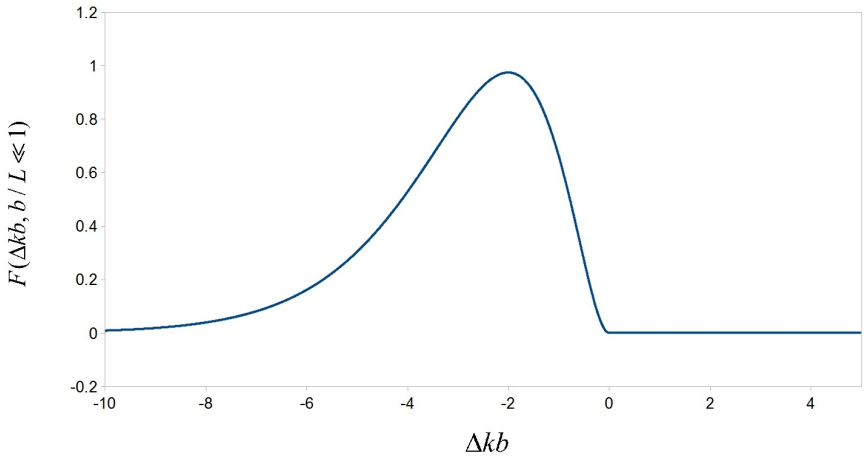

Figure 2.4: A normalized phase matching curve for the case of tight focusing.

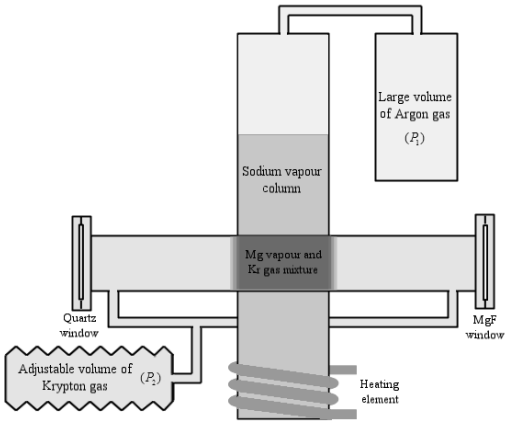

Figure 2.5: Diagram of the crossed heat pipe oven.

Stellenbosch University http://scholar.sun.ac.za

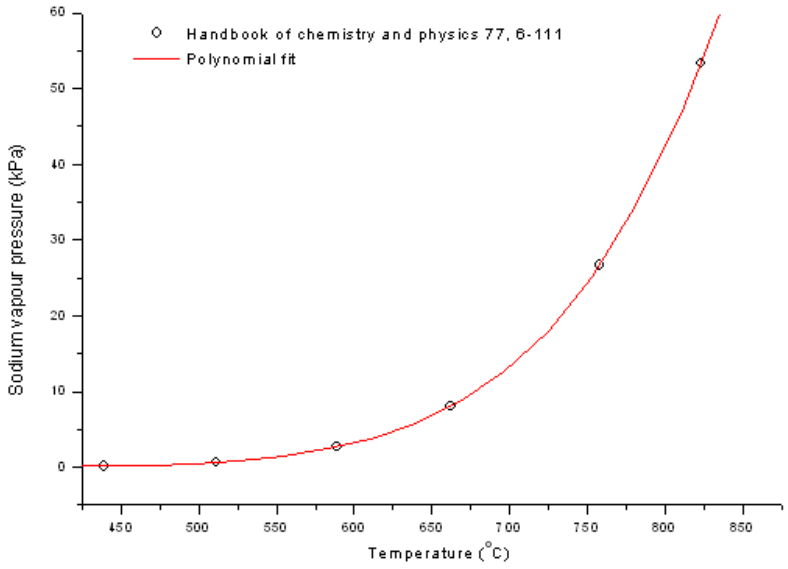

Figure 2.6: Vapour pressure curve of sodium.

with magnesium as working material filled with krypton gas at pressure P_2. The function of the vertical pipe is to provide a very stable homogeneous temperature to immerse the horizontal pipe in. A heating coil is used to heat the vertical pipe near its bottom with constant heating power. The result of heating is the formation of a sodium vapour column. The height of the column is determined by the heating power applied to the coil. A certain minimum power is required for the column to extend past the point of intersection with the horizontal pipe. The temperature of the column is determined by the pressure of the argon gas. Sodium evaporates at its boiling point from the bottom of the heat pipe and condenses again at the top forming a liquid-vapour phase equilibrium. The boiling temperature can be read from the sodium vapour pressure curve shown in figure 2.6, where the sodium vapour pressure is equal to the argon pressure P_1.

The central section of the horizontal pipe is in thermal contact with the sodium vapour column. A magnesium vapour column will form inside the horizontal pipe the density of which is determined by the temperature of the sodium vapour column. The magnesium vapour pressure can be determined from the magnesium vapour pressure curve (figure 2.7) for any given temperature. In order to obtain a magnesium vapour column of sufficient density a temperature of ~ 750 °C is required. The horizontal heat pipe oven is filled with krypton gas at pressure P_2 that must be higher than the magnesium vapour pressure. The krypton gas has two functions. Firstly it helps to confine the magnesium vapour to the central heated section of the heat pipe. Secondly, phase matching is achieved by setting the correct ratio of krypton to magnesium pressure, which yields $n_1 = n_3$ or $\Delta k = 0$.

At the boundary of the vertical heat pipe, where the horizontal pipe passes

Stellenbosch University http://scholar.sun.ac.za

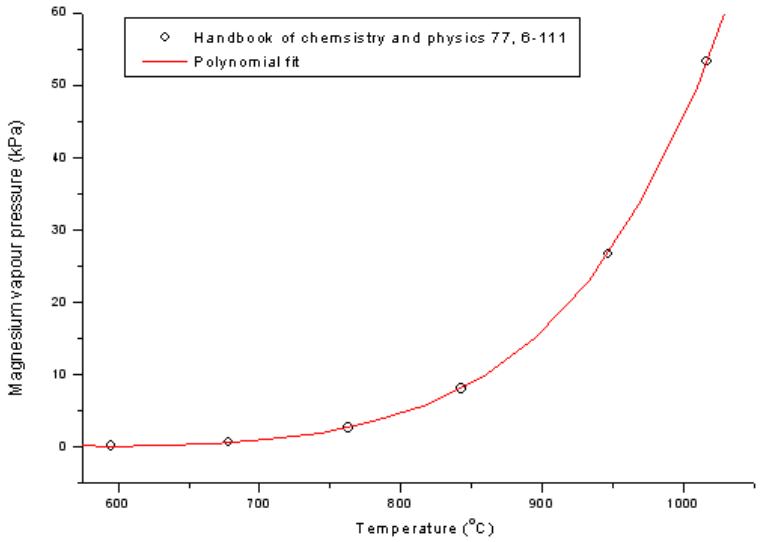

Figure 2.7: Vapour pressure curve of magnesium.

through it to the outside, there is a gradual drop in temperate inside the horizontal pipe as we move away from the heated section. A corresponding gradual drop in the magnesium vapour pressure and increase in krypton pressure will occur in this section, as shown in figure 2.8.

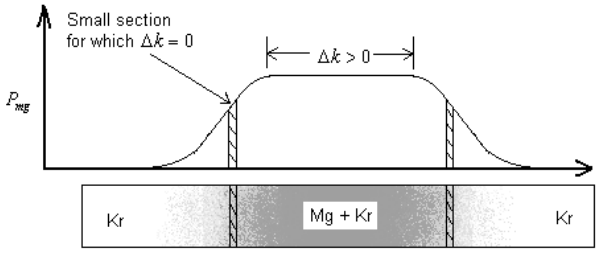

Figure 2.8: Magnesium vapour pressure profile in the horizontal heat pipe shown for the case of $\Delta k > 0$.

Consider the scenario where the ratio of magnesium vapour pressure to krypton pressure in the central heated section is higher than what is required for phase matching i.e. $\Delta k > 0$. As the magnesium vapour pressure drops immediately outside the central heated section a point will be reached where the phase matching condition is satisfied and $\Delta k = 0$. This condition will exist for a small section of the horizontal pipe on both sides immediately outside the central heated section. VUV production will therefore be more efficient within those sections and contribute significantly to the intensity of VUV light produced

Stellenbosch University http://scholar.sun.ac.za

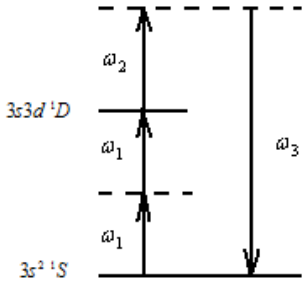

Figure 2.9: Sum frequency generation showing the resonance with the energy levels of Mg, used for the resonant enhancement of $\chi^{(3)}$.

under these conditions.

The magnesium column inside the horizontal pipe is a suitable nonlinear medium for VUV production because it exhibits a high nonlinear susceptibility. It is a centrosymmetric medium meaning that third order nonlinear processes is the lowest order processes that can occur in this medium. Phase matching of the medium is facilitated by the stability and homogeneity of the magnesium vapour which is caused by the stable and homogeneous temperature provided by the sodium equilibrium.

2.1.5 Magnesium vapour as nonlinear medium

Magnesium vapour phase matched with krypton gas has been shown to be an effective nonlinear medium for the production of VUV laser light by Junginger et al in 1980 [12]. They reported a third harmonic conversion efficiency of up to 1.2×10^{-4}. Tunable VUV laser light can be produced by a four wave mixing process depicted in figure 2.9. In order to access the range of wavelengths from 138 to 160 nm we made use of a two-photon resonance with the $3s^2\,^1S - 3s3d\,^1D$ transition. This is achieved by setting the frequency ω_1 to a value were the energy of two of these photons matches with the energy of this transition. In this way the efficiency of the nonlinear process is enhanced. A two photon resonance is most effective as both one- and three photon resonances suffers from absorption of either the fundamental or the VUV photons.

2.2 Spectroscopy of carbon monoxide

2.2.1 Spectroscopic study of carbon monoxide in a supersonic jet

The purpose of the supersonic jet is to prepare the carbon monoxide gas sample for spectroscopic analysis with the tunable VUV laser source. The ideal spectroscopic sample should:

- Comprise an ensemble of molecules all in a particular well defined quantum state, usually the ground state.
- Be traveling in free space with a narrow velocity distribution

Stellenbosch University http://scholar.sun.ac.za

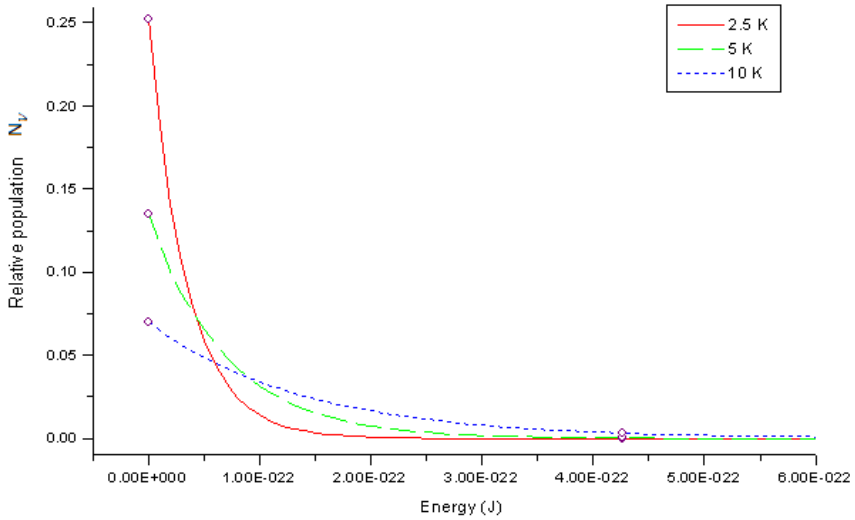

Figure 2.10: Relative population distribution for vibrational levels as a function of energy, shown for three different temperature values. The energies of the v=0 and v=1 states of the $X^1\Sigma^+$ground state of CO are indicated by the open circles.

- Have a sufficiently low collision rate so that intermolecular interactions are unimportant

These requirements can be met to a large degree when the molecules are seeded into a supersonic expansion of a monatomic gas. The translational temperature of a gas in a supersonic expansion falls to extremely low temperatures. During the expansion from high pressure into vacuum the random thermal motion of the gas is converted into directed flow, therefore reducing the velocities of random motion and therefore translational temperature directly.

As monatomic gases do not store energy in vibrational and rotational degrees of freedom, cooling for such gases is more complete than for polyatomic molecules. Carbon monoxide, a diatomic molecule, can be seeded into such an expansion allowing the CO molecules to interact with the low temperature bath provided by the monatomic carrier. Rotational cooling of the CO molecules can be comparable to translational cooling in this kind of expansion, while vibrational cooling tends to be less complete but still quite extensive [13].

The population distribution over the vibrational states of the molecules, N_ν, is given by a Boltzmann distribution, $e^{-E/kT}$, and is a function of energy and temperature [14]. The normalised distribution is plotted as a function of energy for temperatures of 2.5, 5 and 10 Kelvin in figure 2.10. The circles on the graph indicate the energy values for the ground and first vibrational state of the $X^1\Sigma^+$ground state of $^{12}C^{16}O$ on each of the curves. For a temperature of 5 K the population of the first vibrational state will only be 0.21% of that of the ground state. At such low temperatures population of higher vibrational states is therefore negligible. This simplifies the laser induced fluorescence (LIF) spectra obtained from the jet, as only transitions from the ground electronic and

Stellenbosch University http://scholar.sun.ac.za

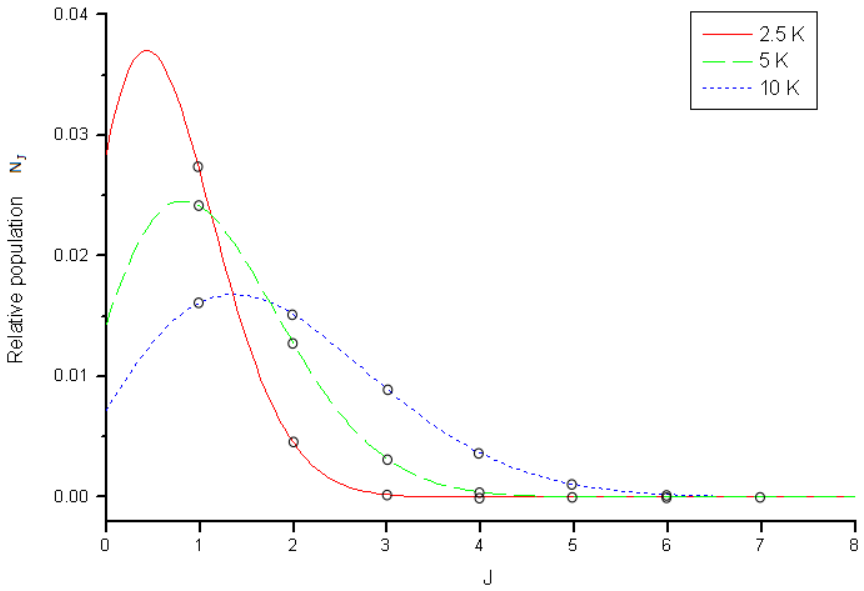

Figure 2.11: Relative populations of rotational energy levels as a function of rotational quantum number J for three different temperature values.

vibrational state to higher vibrational states in the excited electronic state will be observed.

The population distribution over the rotational energy levels, N_J, follows a Maxwell-Boltzmann distribution given by $(2J+1)e^{-BJ(J+1)/kT}$. This is plotted in figure 2.11 for the ground state of $^{12}C^{16}O$ at temperatures of 2.5, 5 and 10 Kelvin respectively. For these temperatures it can be seen from the graph that the levels with the highest populations will be the J = 0, 1, 2 and 3 levels. This means that the strongest spectral lines observed will be lines arising from excitation transitions originating from these levels. Relative intensities of rotational lines can be used to determine the temperature of the CO sample by fitting the Maxwell-Boltzmann distribution to the data.

The main reason for cooling of the CO sample is to simplify the observed spectra. In a sample cooled to 10 K or below, only spectral lines arising from transition from the ground vibrational state and a few of the lowest rotational states are strongly observed. These conditions are similar to those in interstellar gas clouds. We therefore expect to observe the same spectral lines in spectra recorded under these conditions in the laboratory as we do in spectra recorded from interstellar gas clouds, allowing us to accurately identify such lines.

Another advantage of cooling is that it results in the narrowing of spectral lines. The CO molecules in the supersonic expansion are generally all moving in the same direction with a narrow distribution of velocity. For laser induced fluorescence (LIF) spectroscopy we can set up the laser beam to pass through the jet in a perpendicular direction to the motion of the molecules. This limits the effects of Doppler broadening resulting in small spectral line widths.

Stellenbosch University http://scholar.sun.ac.za

2.2.2 The fourth positive system

The fourth positive system of carbon monoxide is a term given to the rovibronic transitions between the singlet electronic ground state, $X^1\Sigma^+$, and the first singlet electronically excited state, $A^1\Pi$. In this study transitions between the vibrational levels $\upsilon' = 3$ of the first excited state and $\upsilon'' = 0$ of the ground state where observed as indicated in figure 2.12. Allowed transitions between rotational energy levels of the upper and lower vibronic states are governed by the selection rule:

$$\Delta J = J' - J'' = 0, \pm 1 \tag{2.17}$$

$$\text{with the restriction } J' = 0 \nrightarrow J'' = 0$$

The selection rules require that the change in angular momentum ΔJ to either be zero, resulting in the Q branch of the spectrum, or change by plus or minus one, resulting in the P and R branches respectively. Figure 2.13 shows the allowed and forbidden transitions for each of the branches in accordance with the selection rule.

The fourth positive system has been characterised by accurate laboratory wavelength measurements for $^{12}C^{16}O$ and $^{13}C^{16}O$ [3], $^{12}C^{18}O$ [15] and $^{12}C^{17}O$ [16].

2.2.3 Singlet-triplet transitions

Electronic transitions are only allowed between individual electronic states having the same spin quantum number S, as indicated by the selection rule:

$$\Delta S = S' - S'' = 0 \tag{2.18}$$

This means that transitions between singlet and triplet electronic states are quantum mechanically forbidden.

There are three triplet electronic states of carbon monoxide whose potential energy curves overlap with that of the $A^1\Pi$ state, namely the $e^3\Sigma^-$, $d^3\Delta$, and $a'^3\Sigma^+$ states. Because of the close vicinity of the singlet and triplet states, mixing occurs between them so that the triplet states obtain some singlet character. This means that although transitions between singlet and pure triplet states are quantum mechanically forbidden, there is a small transition probability between these triplet states and the singlet ground state.

For the singlet-triplet transitions the $\Delta J = 0, \pm 1$ selection rule still applies, giving rise to the P, Q and R branches. However, spin-orbit coupling occurs in the upper triplet state causing the energy levels to split according to their total angular momentum. The transitions are therefore given an additional label, F_1, F_2 or F_3.

Calculated wavelengths for all the singlet-triplet transitions that are of relevance in astrophysics are available. However, accurate laboratory measured wavelengths do not exist for many of the lines [4].

During a previous study in our laboratory a number of singlet-triplet transitions were detected while recording spectra of the $\nu'' = 0$ to $\nu' = 0$, 1, 2, 3, 4, 5 rovibronic bands of the fourth positive system of CO [17]. In the latter study it has been reported that experimental parameters such as the CO fraction in

Stellenbosch University http://scholar.sun.ac.za

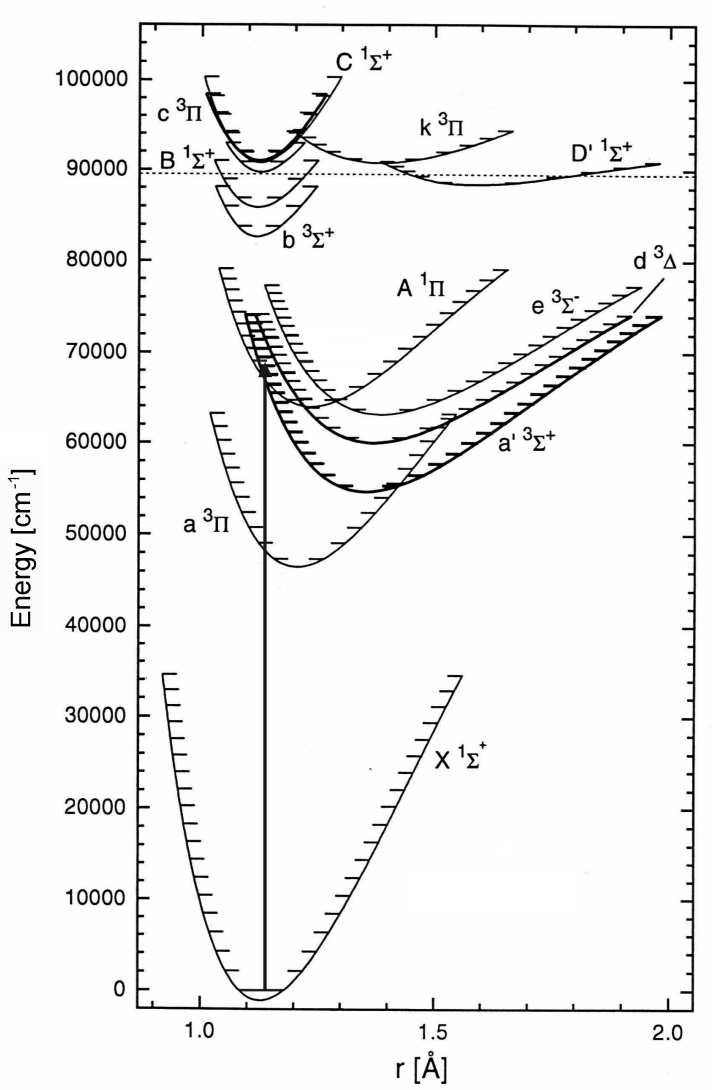

Figure 2.12: Potential energy curves of carbon monoxide, showing electronic and vibrational states. The vertical arrow indicates the $A^1\Pi(v' = 3) - X^1\Sigma^+(v'' = 0)$ vibronic band. This diagram has been calculated by Mellinger [1].

Stellenbosch University http://scholar.sun.ac.za

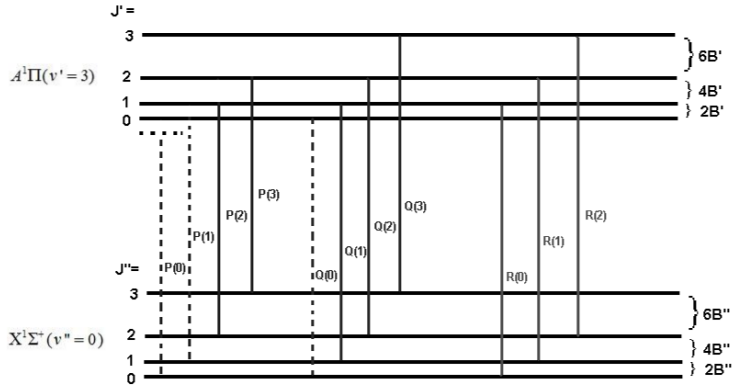

Figure 2.13: Rovibronic transitions between different rovibronic states of $X^1\Sigma^+(\nu''=0)$ and $A^1\Pi(\nu'=3)$. P, Q and R branches are indicated. Allowed transitions are indicated with solid vertical lines and forbidden transitions by dotted lines. B' and B" are the rotational constants of the upper and lower vibrational states respectively.

the supersonic jet, the temporal overlap of the laser pulse in the gas jet and the detection gate setting play important roles in the quality of the spectra and the detection of weak spectral lines. In the experimental study reported here these parameters have been optimised specifically for the detection of the singlet-triplet transitions with the aim of detecting more of the singlet-triplet lines lying close to the $X^1\Sigma^+$ - $A^1\Pi$ band.

Stellenbosch University http://scholar.sun.ac.za

Chapter 3

Experimental setup and optimisation

3.1 Overview of experimental setup

The experimental setup for laser induced fluorescence spectroscopy of carbon monoxide using our tunable VUV laser source is shown in figure 3.1. The setup comprises the tunable VUV laser source, a supersonic jet of CO gas forming the spectroscopic sample, and a system for the detection and recording of the spectra. A brief overview of the components in the experimental setup is given here and the optimisation of these components in terms of the experimental parameters will be discussed in the next section.

An EMG 203 MSC Xe-Cl excimer laser is used to pump two dye lasers (Lambda Physik, FL 3001X). The dye laser beams are co-linearly combined in a polarizing beam combiner (Hablo Optics, PCB 10 M) and focused into a magnesium vapour column inside a heat pipe oven. The dye laser radiation is converted to tunable VUV laser radiation via a four wave sum frequency mixing process inside the magnesium vapour.

For application to spectroscopy of CO the crossed heat pipe is used. The VUV radiation passes into a vacuum chamber and crosses a pulsed supersonic jet containing CO gas. The VUV laser is tuned over a range of wavelengths exiting the CO molecules when the wavelength corresponds to a transition in CO. The total fluorescence from the CO is recorded by a solar blind photo multiplier tube (Hamamatsu R6835) positioned perpendicular to the laser beam and the direction of the jet. A second solar blind photo multiplier tube (Hamamatsu R973) is used to measure the transmitted VUV power and also to record the absorption spectrum. Signals from the photo multiplier tubes are integrated by boxcar integrators (Stanford Research Systems, model SR250) from where they are passed on to a computer interface (Stanford Research Systems, SR 245) that transforms the signals from analogue to digital. The digital signal is received by a personal computer (486 with Windows 3.1) where the data is recorded with the aid of a custom program in HP VEE (Hewlett Packard Visual Engineering).

For the characterisation of the concentric heat pipe, the beam of dye laser II is aligned through the concentric heat pipe. At the exit window of the concentric heat pipe the VUV light passes into a small vacuum system where the VUV

Stellenbosch University http://scholar.sun.ac.za

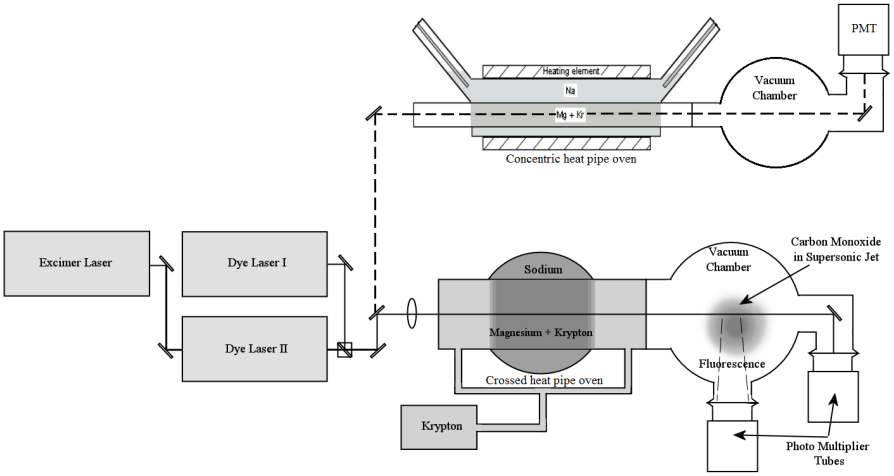

Figure 3.1: Overview of experimental setup. The hardware of the data acquisition system is not shown.

power is measured by a solar blind PMT (Hamamatsu R973) as sketched in figure 3.1.

3.2 Optimization of experimental parameters

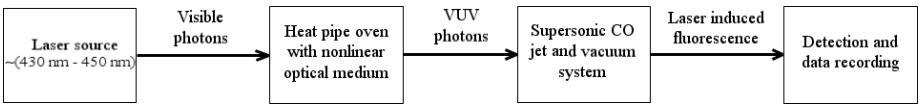

Figure 3.2: Main components of the experimental setup.

The experimental setup for producing tunable vacuum ultraviolet laser light and applying it to the spectroscopy of carbon monoxide is complex and involves many experimental parameters. In this section the setup is divided into four logical components and the setup and parameters of each section is discussed separately. This makes it easier to focus in on what the goal of each component is and how the parameters involved can be optimised to best achieve that goal. Figure 3.2 shows the way this division has been made. The laser source, the heat pipe oven, the supersonic carbon monoxide jet and vacuum system, and the detection and data recording system, make up the four components. Each of these will now be discussed in turn.

Stellenbosch University http://scholar.sun.ac.za

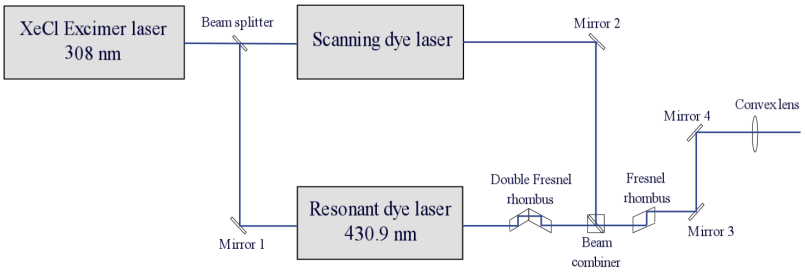

Figure 3.3: The fundamental laser source.

3.2.1 The fundamental laser source

High-intensity narrow-band wavelength tunable light is needed for high-resolution spectroscopic studies. This type of light can be provided by dye lasers that produce tunable laser radiation over a wide spectral region of 330 - 1250 nm. Two dye lasers are therefore used to provide the fundamental frequency photons, that are to be converted to VUV photons through a four wave sum frequency mixing process. The characteristics of the VUV laser pulse, like the bandwidth and pulse duration, is determined by that of the fundamental laser pulses. The dye lasers are pumped by an excimer laser, at 308 nm. This setup is shown in figure 3.3.

One of the dye lasers is tuned to a two photon resonance of Mg at 430.9 nm as discussed in section 2.1.1. This enables us to access a range of wavelengths in the VUV from 140-160 nm. The dye used in the resonant dye laser is Coumarin 440 with a tuning range from 415-470 nm and a good efficiency at the resonant wavelength.

The dye used in the scanning dye laser depends on the wavelength we want to access in the VUV. We investigated the (3,0) band of the $A^1\Pi - X^1\Sigma^+$ transition of carbon monoxide in the wavelength range 144.7 to 145 nm. Coumarin 440 is a suitable dye to use in the scanning dye laser for accessing these wavelengths.

In order to ensure that most of energy from the fundamental laser beams are channeled into the production of tunable VUV laser light, we need to suppress other nonlinear processes that compete for the same energy. There are a number of competing processes the strongest of which is the generation of the third harmonic of the resonant dye laser frequency [6]. As discussed in section 2.1.1 third harmonic generation can be suppressed by giving the two dye laser beams opposing circular polarisations. This is achieved by first passing the beam from the resonant dye laser through a double Fresnel rhombus, changing its polarisation from vertically linear, to horizontally linear. After the beams are combined both are then passed through a single Fresnel rhombus giving the beam from the scanning dye laser a left circular polarisation, and the beam from the resonant dye laser a right circular polarisation. The polarization is never perfect in practice so third harmonic generation always occur to some extent. It is however suppressed to a large extent allowing sum frequency generation to dominate and to be useful as a tunable laser source for spectroscopic application.

Stellenbosch University http://scholar.sun.ac.za

The efficiency of sum frequency generation depends strongly on how well the two dye laser beams overlap in both space and time. Spacial overlapping is achieved in the near field by adjusting mirror 2 (see figure 3.3), and in the far field by adjusting the beam combiner. A fairly good overlap can be achieved by visually overlapping the two laser spots in the near and the far field. Optimization of the overlap can then be done by fine adjustment of the beam combiner while monitoring the intensity of the sum frequency signal on an oscilloscope.

The need for temporal overlap of the beams arises from the pulsed nature of the laser source. This kind overlapping is achieved by ensuring an equal path length for the two beams originating from the splitting of the excimer laser beam. The path length must be equal from the point of splitting by the beam splitter to the point where the dye laser beams are combined by the beam combiner. Because the dye lasers are being pumped by the same source they will then overlap temporally when they pass through the heat pipe.

Examining equation 2.2 we see that the intensity of the produced VUV is proportional to the product of the intensity of the scanning dye laser and the square of the intensity of the resonant dye laser. We can increase the intensity of both these beams locally by focusing them into the magnesium vapour. For focusing a biconvex quartz lens with a focal length of 800 mm was used. A significant increase in the intensity of VUV produced can be obtained in this manner. If the beams are focused too sharply however, VUV production is limited to a small section of the vapour around the focus and we fail to make use of the entire length of the medium.

In the setup for characterisation of the concentric heat pipe by third harmonic generation, the parameters are optimised in a similar way. However, only the resonant dye laser beam is used. The third harmonic power could have been optimised by removing the Fresnel rhombus, but this was not done due to practical considerations.

3.2.2 The concentric heat pipe oven

The heat pipe oven is used to produce the homogeneous magnesium vapour - krypton gas mixture that acts as nonlinear medium for the sum frequency generation process. The operation of the heat pipe is discussed in section 2.1.4. The vapour pressure of the magnesium is determined by the temperature in the heat pipe as can be seen from the vapour pressure curve shown in figure 2.7. In order for the vapour pressure to be high enough for efficient VUV production a temperature of around 750°C is required. Furthermore, any change in the temperature will cause a change in the magnesium vapour pressure and also in the intensity of VUV produced. Fluctuations in temperature during the recording of spectra can therefore result in an inconsistency in the relative intensities observed for spectral lines. We require the temperature in the heat pipe to be very stable in order to produce VUV of constant intensity and not to distort the observed spectra. Thirdly, phase matching throughout the entire length of the magnesium vapour column is only possible if the magnesium vapour pressure is constant for the entire length of the vapour column, which means that we also require the temperature to be uniform over that length. The heat pipe oven provide a simple but effective way to meet both these temperature requirements.

Comparing the designs of the crossed heat pipe, shown in figure 3.4, and the

Stellenbosch University http://scholar.sun.ac.za

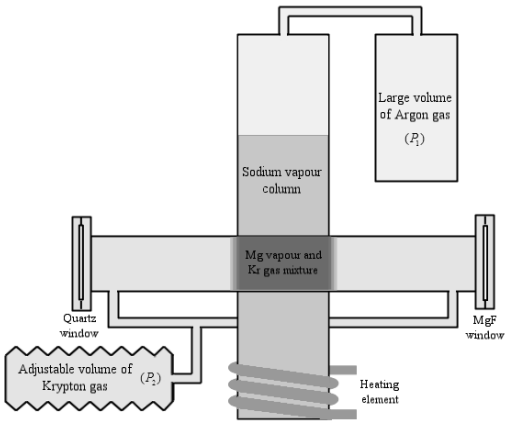

Figure 3.4: The crossed heat pipe oven.

concentric heat pipe, shown in figure 3.5 we note that the operation of the two pipes are the same. In each case a magnesium vapour column is formed inside the section of the inner pipe that is enclosed by the outer pipe containing the sodium vapour. The concentric positioning of the inner pipe inside the outer pipe in the concentric heat pipe ensures that a longer section of the inner pipe is heated forming a longer magnesium vapour column than what is practically possible with a crossed design. The vapour column length is roughly 6 cm for the crossed heat pipe, and 30 cm for the concentric heat pipe. Since the magnesium vapour and Krypton gas mixture forms the nonlinear medium for VUV production a longer vapour column should allow for higher intensities of VUV to be produced.

The two diagonal pipes extending upwards on either side of the concentric heat pipe allows for the sodium vapour column to extend upwards inside these pipes as heating power is increased in much the same way as the sodium vapour column pushes upwards in the vertical pipe of the crossed heat pipe. This is the key to establishing a stable temperature in the concentric heat pipe and what sets it apart from earlier concentric heat pipe designs.

For characterisation and optimisation of the concentric heat pipe the temperature was investigated as a function of the heating power and external Ar pressure respectively. Investigation of the dependence of temperature on heating power was done by setting the heating power to a certain fixed value and allowing the temperature in the heat pipe to reach equilibrium temperature. This happens when a liquid-vapour phase equilibrium is established for the sodium inside the heat pipe, and when the rate at which heat is supplied by the element is matched by the rate at which heat is lost through the walls of the heat pipe. The temperature is measured by thermocouples situated inside the diagonal pipes. The process was then repeated for various values of heating power. For investigation of the dependence of temperature on the external Ar pressure a similar approach was followed and the equilibrium temperature was measured for various values of external pressure.

The phase matching requirement (see section 2.1.2) must be met in order

Stellenbosch University http://scholar.sun.ac.za

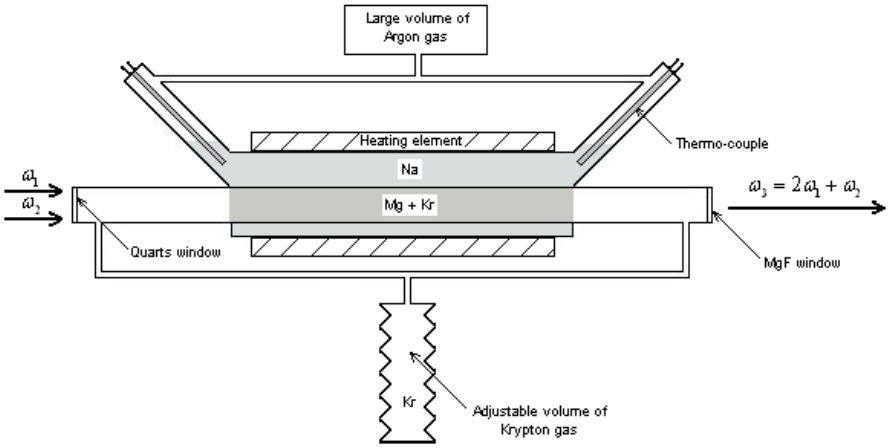

Figure 3.5: A schematic depiction of the concentric heat pipe oven design.

for efficient VUV production to take place. Phase matching can be achieved in a mixture of magnesium vapour and krypton gas, where the pressure ratio, P_{Kr}/P_{Mg}, needs to be around 12.7 [12]. The pressure of the magnesium vapour and the krypton gas have to be independently adjustable. In the heat pipe, shown in figure 3.4 and 3.5, the magnesium vapour pressure is changed by changing the temperature, which is in turn determined by the pressure of the argon gas in the outer pipe. This is usually not adjusted while the heat pipe is in operation but rather set to the desired value before start-up. The krypton gas in the inner heat pipe is connected to an adjustable external volume, allowing the pressure to be changed while the heat pipe is in operation.

Optimal phase matching for sum frequency generation will be achieved at a slightly different Kr pressure from the optimal pressure for third harmonic generation. This can be used to further suppress third harmonic generation. The interval of wavelengths scanned in any one measurement was always small enough so that re-optimization of the phase matching was not required during any measurements.

The dye laser beams pass into the heat pipe through a quartz window whereas the VUV laser light pass from the heat pipe into the vacuum chamber via a magnesium fluoride window. The windows are protected from contamination by using water cooling of the ends of the pipe and baffles with a 5 mm aperture to minimise diffusion of the Mg vapour to the windows.

3.2.3 The supersonic jet and vacuum system for CO spectroscopy

To create a supersonic expansion of gas a chamber containing the CO gas, or CO-Ar gas mixture, at a pressure between 1 and 4 bar is used. The gas chamber is separated from a vacuum chamber by a solenoid pulse valve (General Valve series 9, Part nr. 9-181-900). The valve is controlled by a pulse driver (Iota one pulse driver, General Valve Corporation) which sends a 12 V DC signal of

Stellenbosch University http://scholar.sun.ac.za

a variable length to the valve. The signal passes through a solenoid inside the valve creating a magnetic field which pulls the plunger of the valve open for the duration of the pulse. The length of the pulse is therefore known as the valve on-time. The valve needs to be opened for a certain minimum amount of time in order to allow a sufficient amount of the CO gas mixture to pass through the orifice to provide a spectroscopic sample. The upper limit of the valve on-time is set by the repetition rate of the pulses, and also by the ability of the vacuum pumps to recover the vacuum between subsequent gas pulses. A repetition rate of 5 Hz was used throughout during spectroscopic measurements. The valve releases the gas mixture into the vacuum chamber held at a pressure of around 10^{-5} mbar with a turbo molecular pump (Pfeiffer TPH 200, 190 ℓ/s) backed by a rotation pump (Vacuubrand, model RS-15, 15 m^3/h). The pressure is measured by two pressure transducers, a Pirani model 162 02 B2, and a Penning model 172 85 B1, both from Leybold-Heraeus.

In some cases a mixture of CO and Argon gas, and in other cases pure CO was used when recording spectra. When Ar gas is present it acts as a monatomic carier gas facilitating cooling in the jet, causing it to reach a lower temperature than with pure CO. On the other hand, using pure CO increases the signals of lines with low transition probabilities like singlet-triplet transitions. The temperature in the jet for a pure CO sample still drops below 10 Kelvin . We can make the approximation that all CO molecules will be in the ground electronic energy level at this temperature [13].

3.2.4 Detection and data recording

3.2.4.1 Photo-multiplier tubes

Both laser induced fluorescence (LIF) and the transmitted VUV light (absorption spectra) are recorded in this experiment. These spectra all lie in the VUV region of the spectrum and solar blind photo-multiplier tubes (PMT's) are used to detect the VUV photons. This means that photons in the visible region of the spectrum like scattering of the dye laser beams will not be registered by the PMT's so that the LIF spectra are background free.

Two similar models of solar blind PMT's from the Hamamatsu company was used, the R6835, and the R973. Both have a layer of Ce-I on the entry window that act as a semi-transparent photo-cathode with a peak sensitivity at 140 nm. The quantum efficiency of this material is shown in figure 3.6 (a). A high negative voltage, usually -2 kV, is applied to the cathode and the anode is grounded through a load resistor.

Figure 3.6 (b) shows the gain of the PMT as a function of the supply voltage. The high amplification attainable makes a PMT an extremely sensitive detection apparatus. This is important as the conversion efficiency from the visible dye laser photons into VUV photons is small yielding low VUV intensities, in spite of careful optimization discussed in section 3.2.2. The laser induced fluorescence from the CO gas is of even lower intensity requiring a sensitive detection instrument like a PMT.

3.2.4.2 The boxcar integrators

Both the PMT detecting the fluorescence and the PMT detecting the transmitted VUV light are connected to Boxcar integrators (Stanford research systems,

Stellenbosch University http://scholar.sun.ac.za

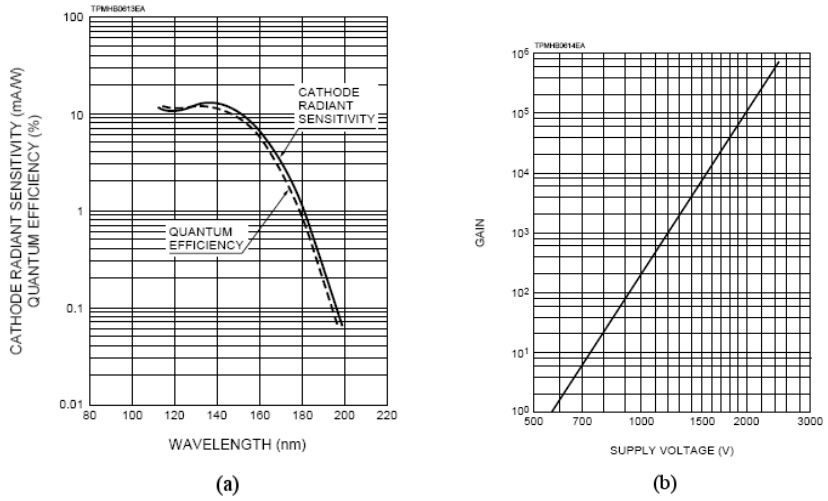

Figure 3.6: (a) Typical spectral response and (b) gain characteristics for the Hamamatsu R6835 photo multiplier tube [2].

model SR250). The boxcar measures the potential difference over time across the load resistor of the PMT and integrates over a certain portion of this signal, as specified by the delay and width of the boxcar gate. The delay is measured from the time the boxcar receives a trigger signal from a photo-diode. The diode is placed so that it will intercept a small portion of light from the excimer laser beam, after that beam has passed through the resonant dye laser. The width of the boxcar gate determines the length of the integration time over the signal.

In most cases the width and delay of the gate needs to be set in such a way as to optimise the signal to noise ratio in the detected VUV or fluorescence signal. This can be done by viewing both the signal from the PMT and the boxcar gate on an oscilloscope and visually overlapping the gate with the peak of the signal. This is depicted graphically in figure 3.7, where t_0 marks the arrival time of the trigger signal, and t_1 and t_2 the start and end time for integration respectively. Further optimisation of these settings can be done experimentally by measuring the effect of the settings on the signal to noise ratio of recorded spectra.

3.2.4.3 Computer control and data recording

The output from the boxcars are digitised by a computer interface and the data transferred to a 486 personal computer running Windows 3.1. A custom program in HP Vee (Hewlett Packard Visual Engineering Environment) is used to record the data and to execute control over the experiment. In order to improve the signal to noise ratio the average of the signals of ten laser pulses are usually taken for one data point recorded by the computer. In cases where very low intensity lines are being observed the average of thirty or a hundred signals can be taken. Unfortunately this slows down the recording process and limits the range of wavelengths that can practically be covered in one scan.

The flow of control commands and trigger signals between the various components of the data recording setup is depicted in figure 3.8. When a wavelength

Stellenbosch University http://scholar.sun.ac.za

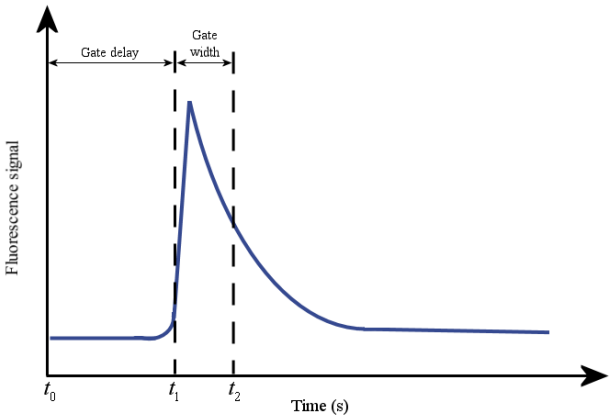

Figure 3.7: Visual setup of boxcar gate and delay over an observed fluorescence signal on the oscilloscope.

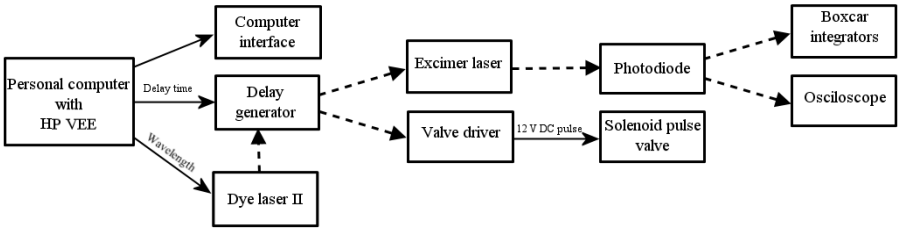

Figure 3.8: The flow of control commands and trigger signals. Solid lines represent control signals and dashed lines represent trigger signals.

Stellenbosch University http://scholar.sun.ac.za

scan is started, the computer communicates with the scanning dye laser commanding it to set the grating to the correct position according to the initial wavelength, also specifying the grating order that is to be utilised. Once the dye laser grating is in position the computer commands the dye laser to send a trigger signal, which is received by the delay generator. The computer also communicates directly with the delay generator in order to set the delay time to the value set by the user. The delay generator first sends a trigger signal to the driver of the pulse valve that opens the valve releasing a pulse of CO gas into the vacuum chamber. After the specified delay time, the delay generator then sends a trigger signal to the excimer laser. The optimal delay time is determined experimentally by performing delay scans, where the fluorescence signal from a specific transition of CO is plotted as a function of the delay time. When the excimer beam reaches the photo-diode the resulting signal from the diode acts as a trigger for the boxcar systems. The two boxcars then integrate over a certain portion of the signals from the PMT's according to each boxcar's own delay and width settings. The result of the integration is then passed on to the computer for recording. This is repeated for the chosen number of laser pulses and the average taken over the ten resulting samples before the computer commands the dye laser to move onto the next wavelength setting.

The laser induced fluorescence and VUV laser photons are detected by the two solar-blind PMT's. Figure 3.9 shows how this data is passed on through the system until it is recorded by the computer. Photons resulting from laser induced fluorescence in the CO gas that reach the entry window of the PMT cause electrons to be ejected from the photo-sensitive Cs-I layer. These electrons form an electronic signal proportional in strength to the intensity of the fluorescence. The electrons are accelerated by the electric fields inside the PMT and amplified at each of the dynodes. The amplified current finally flows through the load resistor causing a voltage difference that is measured by the boxcar integrator. The same chain of events take place for the VUV laser photons observed by the other PMT.

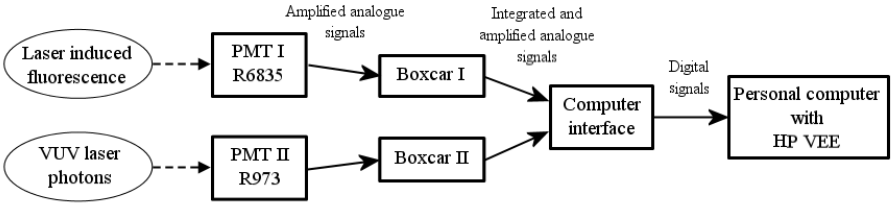

Figure 3.9: The flow of data from the photo multiplier tubes to the computer.

The boxcars integrate these signals and amplify them further after which they are passed on to the computer interface as analogue signals. The computer interface converts the signals from analogue to digital and passes them on to the computer where averaging and recording takes place.

Stellenbosch University http://scholar.sun.ac.za

Chapter 4

Experimental results and discussion

4.1 Characterisation of the VUV source using a concentric heat pipe oven

In this section the experimental characterisation of the VUV source is discussed firstly in terms of the thermal characteristics of the concentric heat pipe oven and then in terms of the characteristics of the generated VUV output. For thermal characterisation the equilibrium temperature in the concentric heat pipe was investigated as a function of heating power and as a function of the pressure of the external argon gas.

Characterization of the VUV output involves the investigation of the effect of the two photon resonance in magnesium and phase matching, as well as the intensity of the VUV source.

4.1.1 Thermal characteristics of the heat pipe oven

The ability of the concentric heat pipe oven to produce a metal vapour column of stable temperature under varying heating power was investigated in experiment. Temperature measurements were taken with the heat pipe set to various heating powers with the external Ar pressure constant at 8 kPa. The result of these measurements for six different heating powers is shown in figure 4.1.

The lowest heating power that was used is 740 W, for which a temperature of 300 °C was recorded. For the next two values of heating power investigated, namely 875 and 1040 W, a steady increase in temperature is observed. Any further increase in the heating power did not produce a significant change in the observed temperature. This behavior can be explained by looking at the position of the thermo-couples measuring the temperature in the heat pipe (figure 3.5). The heating power is not expected to have a direct effect on the temperature of the Na vapour in the heat pipe but only on the height of the column of Na vapour. For low heating powers the vapour column does not reach the tip of the thermo-couple and a lower temperature is recorded than would have been expected as equilibrium temperature for the given Ar gas pressure. As the heating power is increased the vapour column pushes past the tip of the

Stellenbosch University http://scholar.sun.ac.za

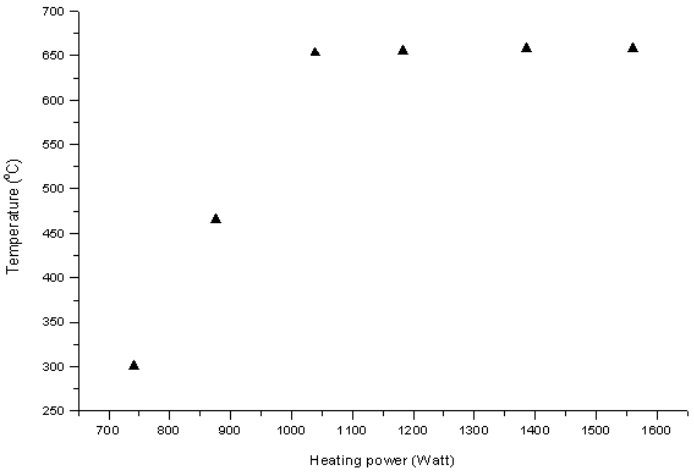

Figure 4.1: Temperature versus heating power for the concentric heat pipe. This was recorded at an Ar pressure of 8 kPa.

thermo-couple allowing the true equilibrium temperature to be recorded. This occurs at a heating power of around 1040 Watt, where a temperature of 653 °C was measured. Any further increase in the heating power did not produce a significant change in the observed temperature. This shows that the concentric heat pipe produces a vapour column with a stable temperature that is not affected by variations in the heating power, providing that a certain minimum is exceeded.

To show the dependence of temperature inside the heat pipe on the external argon pressure, temperature measurements where taken at various Ar pressures. The results are shown in figure 4.2. These measurements where taken at a constant heating power of 1560 Watt. As can be seen from figure 4.1 this is enough power to produce a vapour column high enough to engulf the tip of the thermo couple where the temperature measurement is taken. The temperature measured can therefore be trusted to be the equilibrium temperature.

The results show a good correlation to the values expected at the various pressures as predicted by the vapour pressure curve of sodium. A small deviation is observed however, especially for pressure values over 10 kPa. The most likely cause for this is an inaccuracy in the calibration of the pressure gauge or the thermocouple temperature readout.

4.1.2 The two photon resonance

The effectiveness of using a two photon resonance of Mg to enhance the efficiency of third harmonic generation was investigated experimentally. The wavelength of dye laser I was varied in steps of 1 pm from 430.889 nm to 431 nm while the intensity of the third harmonic signal was recorded with a solar blind photo-multiplier tube. The pulse energy of the dye laser was ~ 1.3 mJ and the beam was focused with a 2000 mm focal length lens. The result of this measurement is shown in figure 4.3.

Stellenbosch University http://scholar.sun.ac.za

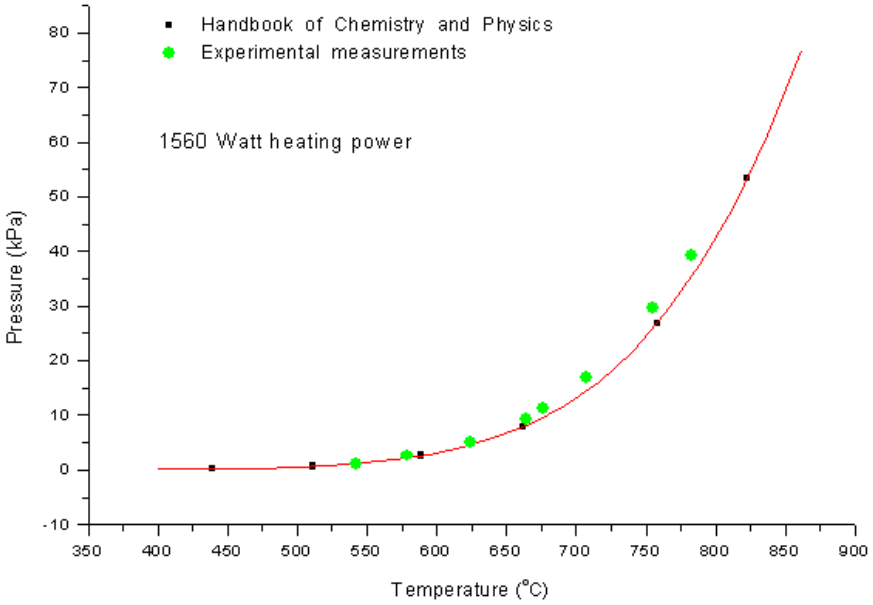

Figure 4.2: Points on the sodium vapour pressure curve as measured with the concentric heat pipe oven compared to values from the Handbook of Chemistry and Physics.

Far from the resonance wavelength no third harmonic signal was observed. Blocking and then unblocking the laser beam at these wavelengths produced no change in the signal recorded by the photo multiplier tube. Whilst we suspect that some third harmonic signal must be generated away from the resonance the intensity appears to be too low to be observed. A sharp increase in the signal was observed around the resonant wavelength with a peak at 430.927 nm. The full width at half maximum of the peak is 0.007 nm.

This shows the importance of using the two photon resonance to enhance the non linear optical susceptibility for third harmonic generation. Without this enhancement the intensity of the tunable laser source would be too low to be useful as a source for laser induced fluorescence spectroscopy.

4.1.3 Phase matching

A phase matching curve was recorded for the concentric heat pipe oven by varying the krypton pressure from 27.0 kPa to 20.7 kPa in steps of 0.1 kPa. The temperature inside the heat pipe was 730 °C when the measurements were taken resulting in a Mg vapour pressure of 1.9 ± 0.5 kPa. A 2000 mm focal length lens was used to focus the laser beam into the heat pipe. The result of the measurement is shown in figure 4.4.

A prominent peak in the third harmonic signal is observed at a Kr pressure of 24.4 ± 0.5 kPa where the ratio of Kr pressure to Mg vapour pressure is 12.8 ± 0.5. The peak occurs where the wave vector mismatch $\Delta k = 0$. As the krypton pressure was decreased from this value an oscillatory structure was observed in

Stellenbosch University http://scholar.sun.ac.za

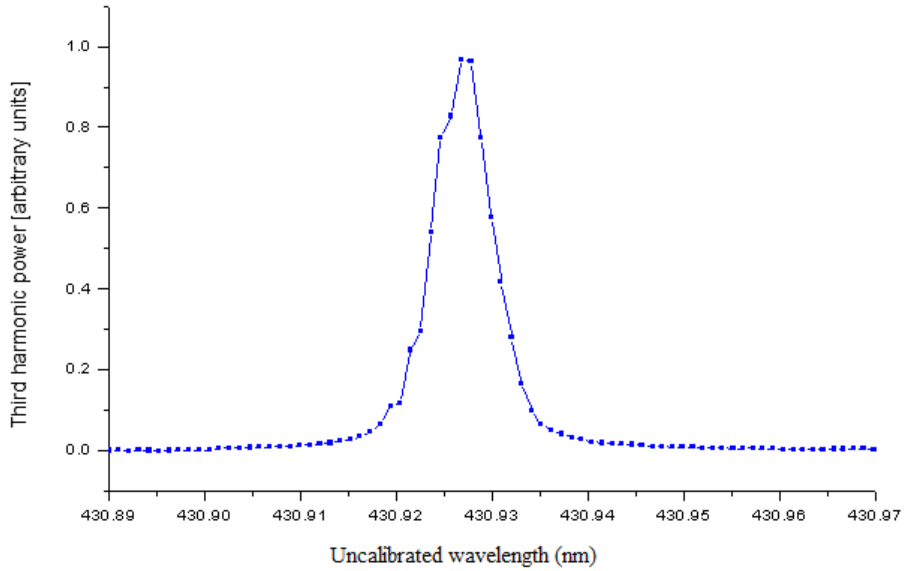

Figure 4.3: Third harmonic signal intensity versus wavelength of the resonant dye laser, showing a sharp increase at the resonant value.

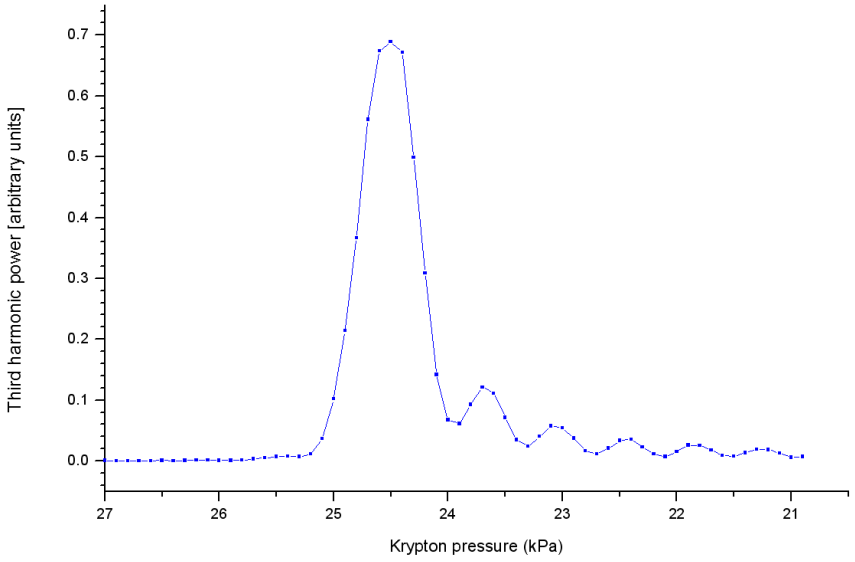

Figure 4.4: A phase matching curve for the concentric heat pipe oven with a medium length of $\sim$ 30 cm. The temperature inside the heat pipe was 730 °C and a 200 cm focal length lens was used to focus the incoming dye laser beam.

Stellenbosch University http://scholar.sun.ac.za

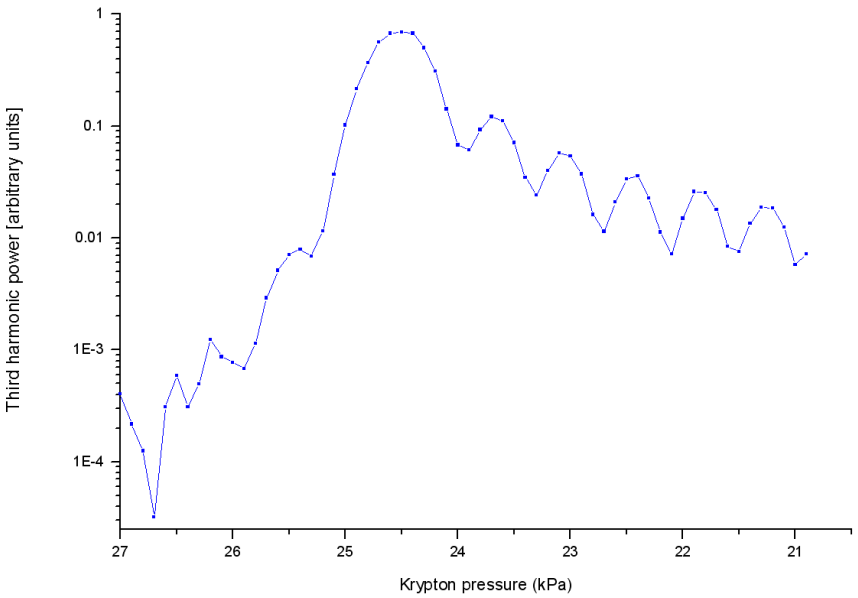

Figure 4.5: Phase matching curve from 4.4 shown on a logarithmic scale.

the third harmonic signal. This matches with the oscillatory structure predicted by the equation for the phase matching factor as shown in figure 2.1. The phase matching curve is however asymmetrical with the oscillatory structure being much more pronounced on the side of the peak corresponding to negative wave vector mismatch values, i.e. towards the lower Kr pressure side of the curve (the right hand side)[1].

This can be understood by considering the Mg vapour density profile in the heat pipe as illustrated in figure 2.8. When the ratio of Kr to Mg pressure in the central part of the heat pipe is too low for phase matching (right hand side of the maximum in figure 4.4) there will be a small section immediately outside the heated section where the Mg pressure is lower and the phase matching condition is met (see figure 2.8). This contributes significantly to the resulting third harmonic intensity on the lower Kr pressure side of the main peak. When the Kr to Mg pressure ratio is too high for phase matching (left hand side of maximum in figure 4.4), the phase matching condition is not met anywhere in the medium and the third harmonic intensity is low. When plotting the phase matching curve on a log scale, as done in figure 4.5, it is possible to discern only the first secondary maximum on the higher Kr pressure side of the curve before it gives way to noise.

Phase matching curves were recorded using both the concentric heat pipe and the crossed heat pipe ovens, producing medium lengths of approximately 30 cm and 6 cm respectively. In order to be able to compare these curves both

[1] Note that all phase matching curves are plotted with decreasing krypton pressure on the x-axis.

Stellenbosch University http://scholar.sun.ac.za

were recorded without the use of a focusing lens. Figure 4.6 shows the result of these measurements for (a) the concentric heat pipe, and (b) the crossed heat pipe.

Comparing the width of the peaks for the phase matching curves of the respective heat pipes, we notice that for the concentric heat pipe the peaks are much narrower. This is what we expect from the theoretical dependence of the phase matching factor $F(\Delta k, L)$ on the length of the nonlinear medium, as shown in figure 2.1. We quantify this by observing the spacing between consecutive minima for both curves. For the concentric heat pipe we have an average spacing of 0.63 kPa and for the crossed heat pipe an average spacing of 3.93 kPa. The ratio of these values is 6.24 which serves as an indication of the ratio of the lengths of the magnesium vapour columns in the respective heat pipes. This is slightly larger than the ratio we get by comparing the lengths of the externally heated sections of the heat pipes which is 30 cm and 6 cm respectively giving a ratio of 5.

Because the peak at $\Delta k = 0$ is much narrower for the concentric heat pipe it is crucial to ensure that phase matching is optimised when using this heat pipe, as the intensity of the VUV laser light produced drops sharply the Kr pressure differs from the optimum value by as little as 0.5 kPa.

The modulation depth of a phase matching curve can be determined by taking the ratio of curves fitted through the maxima and minima respectively (See figure 2.3). This has been done for the phase matching curve shown in figure 4.7 recorded at a temperature of 730 °C. Taking the average ratio of the two curves we get M = 6.70 as the modulation depth. This can be related back to the optical depth via equation 2.12 and a value of $\Gamma_s = 1.63$ is obtained. This is smaller than the value of $\Gamma_s = 2.2$ obtained by Steffes et al [11] for a phase matching curve recorded at a similar temperature of 728 °C.

The effect of focusing on phase matching was investigated by measuring phase matching curves with different degrees of focusing applied to the incoming laser beams. Phase matching curves were recorded with focusing lenses of 750 mm and 1000 mm focal length. The result is shown in figure 4.8 together with a phase matching curve recorded without the use of any focusing. The peak of the curve is noted to shift to lower Kr pressures as the focusing of the incoming laser beam is increased. This is explained by non-parallel wave components present in the focused beam satisfying the phase matching condition for small negative values of Δk, making a noticeable contribution to the amount of VUV laser light produced.

The shift of the phase matching peak towards negative delta k values was calculated in theory for the tight focusing limit only as discussed in detail in section 2.1.3. The experimental results presented here demonstrates the continuous transition between the parallel beam limit (without lens) and conditions approaching tight focusing (750 mm lens).

It is also evident from the figure that an increase in focusing causes a reduction of the modulation depth of the phase matching curve. This is due to the presence of multiple laser modes within the beam each of which is expected to have a significantly different phase matching curve [8]. As a result the oscillatory structure is smeared out to a large degree.

Stellenbosch University http://scholar.sun.ac.za

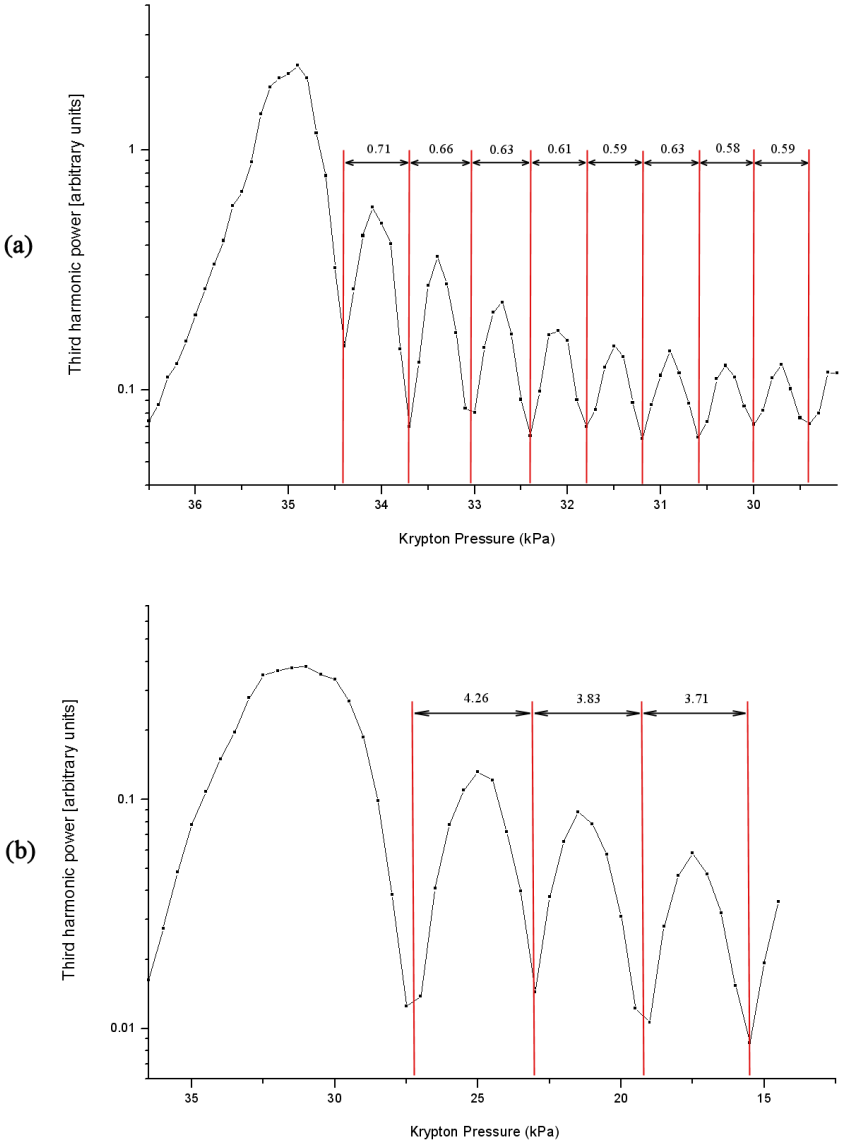

Figure 4.6: Phase matching curves recorded with an unfocused beam for (a) the concentric heat pipe with medium length $\sim$ 30 cm at 730°C, and (b) the crossed heat pipe with medium length $\sim$ 6 cm at 710 °C.

Stellenbosch University http://scholar.sun.ac.za

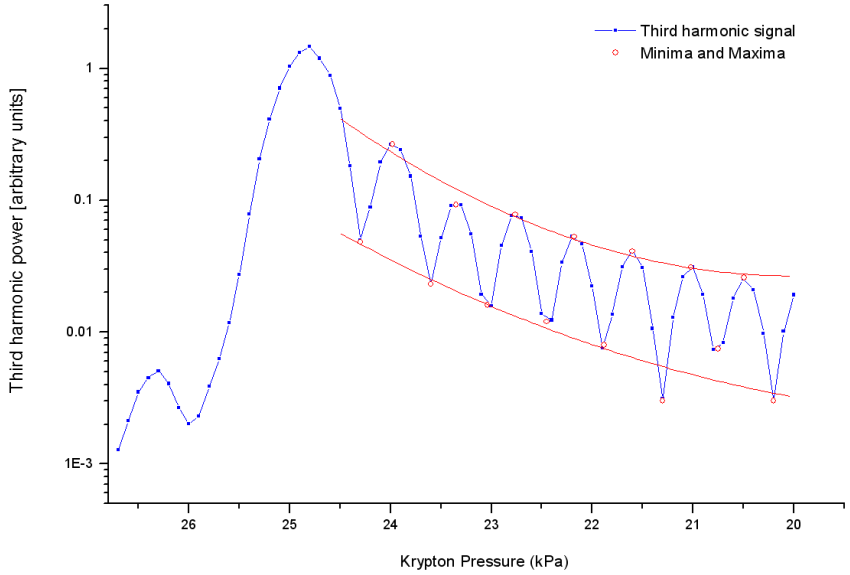

Figure 4.7: The modulation depth in a phase matching curve for the concentric heat pipe with medium length $\sim$ 30 cm. The incoming beam is unfocused and the temperature in the heat pipe was 730 °C.

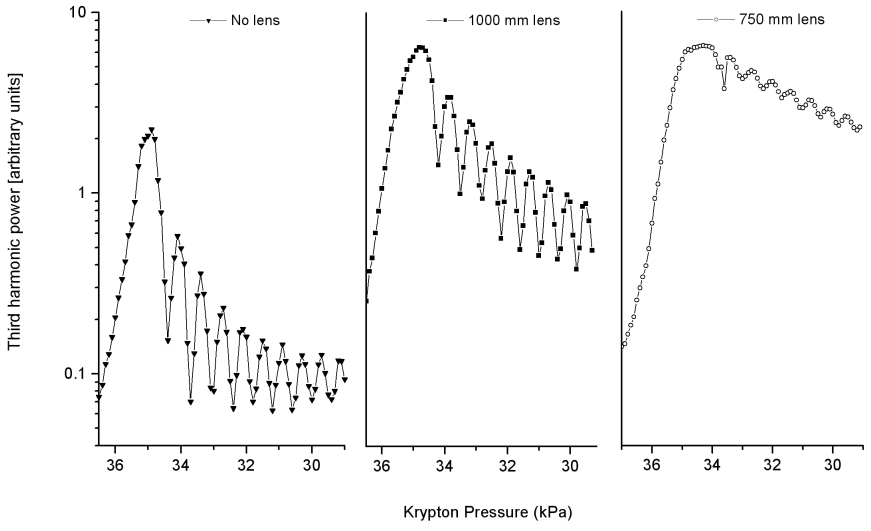

Figure 4.8: Phase matching curves recorded for the concentric heat pipe with different degrees of focusing applied to the incoming laser beam. Medium length was $\sim$ 30 cm and the temperature inside the heat pipe was 730°C.

Stellenbosch University http://scholar.sun.ac.za

4.1.4 Intensity

For the purposes of comparing phase matching curves, especially in terms of the peak intensities, it would be ideal to have equal temperatures inside the heat pipes at the time of recording the curves. This is difficult to achieve in practice as the Ar pressure changes during the heating up process resulting in a change in the equilibrium temperature. When recording the phase matching curves shown in figure 4.6 the Ar pressures for the crossed and concentric heat pipes were 27.0 and 29.3 kPa respectively. Consulting the vapour pressure curve of Na we see that this will result in equilibrium temperatures of 759 and 766°C, with a temperature difference of ~7°C or 1%. Whilst this is a small change in temperature it can have a significant effect on the Mg vapour pressure. According to the Mg vapour pressure curve this amounts to Mg vapour pressures of 2.6 ± 0.5 and 2.8 ± 0.5 kPa, with a pressure difference of 0.2 kPa or 7.7%.

The higher Mg pressure in the concentric heat pipe means that the phase matching condition $\Delta k = 0$ will be met at a higher Kr pressure. This is evident in figure 4.6 where the peak of the phase matching curve for the concentric heat pipe occurs at 34.9 ± 0.5 kPa but for the crossed heat pipe occurs at 31.3 ± 0.5 kPa. The respective Kr/Mg ratios at these pressures are12.5 ± 0.5 and 12.0 ± 0.5, which agree when the accuracy of the values are taken into account.

The peaks of the phase matching curves represent the peak output intensity of the heat pipe ovens for the given input intensity and focusing conditions. Comparing the signals recorded by the photo multiplier tube in arbitrary units of power the peak of the phase matching curves for the crossed and concentric heat pipes were 0.38 and 2.23 respectively. In both cases the energy per pulse from the dye laser was at 1.2 mJ and no focusing was applied. The peak power for the concentric heat pipe was 5.9 times higher than for the crossed heat pipe.

The factors that influence the ratio of the VUV intensity generated in the crossed and concentric heat pipes, I_{cross} and I_{conc} respectively, are the different values for the third order susceptibilities, $\chi^{(3)}$, due to different medium densities N, the difference in medium length L and the difference in intensity of the fundamental laser beam I'.

In the experimental setup incorporating the concentric heat pipe the path length of the dye laser beam from the beam waist inside the laser to where it enters the heat pipe is ~ 5 m. For the crossed heat pipe this path length is only ~ 3.5 m. Because of the divergence of the beam its intensity at the point where it enters the concentric heat pipe will be lower than the intensity at the point where it enters the crossed heat pipe by a factor $\frac{3.5}{5}$. This will negatively affect the production of VUV in the concentric heat pipe. To estimate the effect of the lower fundamental intensity, the medium length and the difference in magnesium vapour pressure we refer to equation 2.2 to get an expression for the ratio of VUV intensities for the concentric and crossed heat pipes in terms of the ratios of these parameters

$$\frac{I_{conc}}{I_{cross}} = \left(\frac{\chi^{(3)}_{conc}}{\chi^{(3)}_{cross}}\right)^2 \left(\frac{L_{conc}}{L_{cross}}\right)^2 \left(\frac{I'_{conc}}{I'_{cross}}\right)^3$$

Where $\chi^{(3)}$ is the third order susceptibility, I' is the intensity of the incoming dye laser beam in each case, and L is the lengths of nonlinear media inside the

Stellenbosch University http://scholar.sun.ac.za

heat pipes. By using $I' = \frac{P'}{A}$, and the fact that the susceptibility is proportional to the magnesium particle density N we get

$$\frac{I_{conc}}{I_{cross}} = \left(\frac{N_{conc}}{N_{cross}}\right)^2 \left(\frac{L_{conc}}{L_{cross}}\right)^2 \left(\frac{P'_{conc}}{P'_{cross}}\right)^3 \left(\frac{A'_{cross}}{A'_{conc}}\right)^3$$

where P' is the power of the incoming beam and A' is the surface area of the fundamental beam at the point where it enters the respective heat pipes. Assuming that $P'_{conc} \approx P'_{cross}$ and noting that the area of the beam increases with the square of the beam radius r we get

$$\frac{I_{conc}}{I_{cross}} = \left(\frac{N_{conc}}{N_{cross}}\right)^2 \left(\frac{L_{conc}}{L_{cross}}\right)^2 \left(\frac{r^2_{cross}}{r^2_{conc}}\right)^3$$

Because the photomultiplier tube measures power rather than intensity we can convert this to the ratio of the VUV power by multiplying with the area of the VUV beam A. We use the estimate that

$$\frac{A_{conc}}{A_{cross}} \approx \frac{A'_{conc}}{A'_{cross}} = \frac{r^2_{conc}}{r^2_{cross}}$$

This yields

$$\frac{P_{conc}}{P_{cross}} = \left(\frac{N_{conc}}{N_{cross}}\right)^2 \left(\frac{L_{conc}}{L_{cross}}\right)^2 \left(\frac{r^2_{cross}}{r^2_{conc}}\right)^3 \left(\frac{r^2_{conc}}{r^2_{cross}}\right)$$

$$= \left(\frac{N_{conc}}{N_{cross}}\right)^2 \left(\frac{L_{conc}}{L_{cross}}\right)^2 \left(\frac{r_{cross}}{r_{conc}}\right)^4$$

Substituting values for L, r and the magnesium vapour pressure, this becomes

$$\frac{P_{conc}}{P_{cross}} = \left(\frac{2.8}{2.6}\right)^2 \left(\frac{30}{6}\right)^2 \left(\frac{3.5}{5}\right)^4$$

$$= 7$$

As a rough estimate of the expected power ratio this factor of 7 compares well with the value of 5.9 obtained.

Importantly focusing the incoming laser beam increases the intensity of the beam inside the nonlinear medium. This can have a significant effect on the

Stellenbosch University http://scholar.sun.ac.za

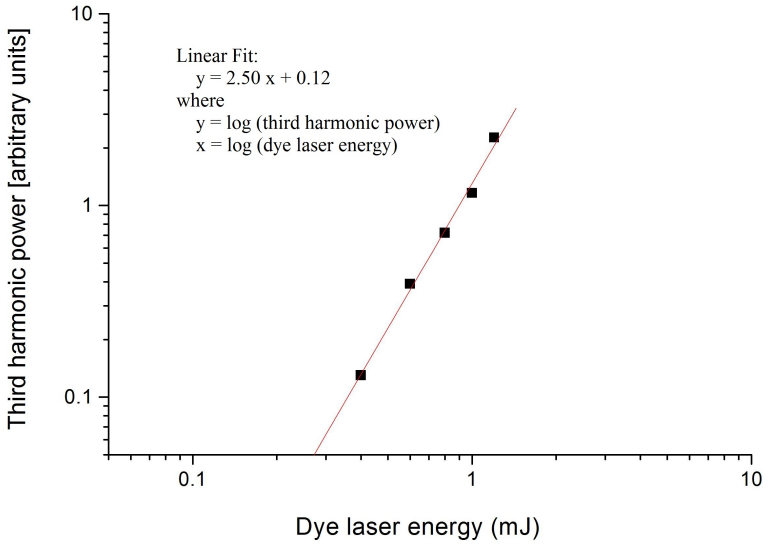

Figure 4.9: VUV laser output power versus input energy from the dye lasers plotted on a double logarithmic scale.

intensity of the VUV laser light produced. With the concentric heat pipe the peak intensity in arbitrary power units observed with no focusing of the incoming beam is 2.24. When using the 1000 mm and 750 mm lenses the peak powers were 6.47 and 6.49 respectively. The small difference between the last two peak powers indicates that using a 750 mm lens is close to optimal focusing for gaining as high an output intensity as possible. Such optimal focusing condition is reached approximately when the confocal parameter is equal to the medium length. Tighter focus does increase the intensity at the focus, but reduces the length of the focal region so that only a fraction of the medium length is used efficiently.

The peak power of the third harmonic signal was measured as a function of the energy of the incoming dye laser beam for five different energy values. The results are shown in figure 4.9, where a linear fit through the data points have also been made. Theoretically the power of the output from a third order non-linear optical process should be related to the incident laser energy by $log(third\ harmonic\ power) = 3\ log(dye\ laser\ energy)$. However, the gradient of the linear fit is only 2.5. Most likely this is due the fact that as the energy increases we move further away from the small signal limit, and the approximations made for the small signal limit are less accurate.

Stellenbosch University http://scholar.sun.ac.za

Isotopomer	Natural abundance (%)
$^{12}C^{16}O$	98.668
$^{13}C^{16}O$	1.100
$^{12}C^{18}O$	1.979×10^{-1}
$^{12}C^{17}O$	3.790×10^{-2}
$^{13}C^{18}O$	2.207×10^{-3}
$^{13}C^{17}O$	4.224×10^{-4}

Table 4.1: Natural abundance of the stable isotopomers of CO.

4.2 Spectroscopy of carbon monoxide

4.2.1 Spectrum of $^{12}C^{16}O$, $^{13}C^{16}O$ and $^{12}C^{18}O$

The stable isotopomers of CO occur with natural abundances indicated in table 4.1. In a typical spectrum recorded during this study of the $A^1\Pi(v = 3) - X^1\Sigma^+(v = 0)$ vibronic band, spectral lines are observed for the three most abundant isotopomers. An example of such a spectrum is shown in figure 4.10. The spectrum covers the spectral region of the band head and band origin of $^{13}C^{16}O$ and $^{12}C^{18}O$. Only higher J lines of $^{12}C^{16}O$ are present. The band origins of $^{12}C^{16}O$ and $^{12}C^{17}O$ fall towards the short wavelength side outside the wavelength range of this spectrum. The fact that lines from $^{12}C^{18}O$ can be observed (for example the Q3 and Q4 lines that can be resolved individually) despite its low natural abundance of only $\sim 0.2\%$ is a good indication of the sensitivity of the measurement. Lines from the even less abundant $^{12}C^{17}O$ isotopomer have also previously been observed in this laboratory [18, 16], but not in the present study.

4.2.2 Calibration of spectra

Each measured spectrum was individually calibrated by using wavelength values for the $^{12}C^{16}O$ and $^{13}C^{16}O$ singlet-singlet lines from Morton and Noreau [3]. A typical fit used to determine the calibration function is shown in figure 4.11. The accuracy of the wavelength values listed by [3] are determined by the accuracy of the upper state term values used in their calculation, which is stated to be approximately 0.1 cm^{-1}. The standard deviation of the difference between the calibrated observed wavelengths and the corresponding literature values is 1.7×10^{-4} nm, corresponding to 0.09 cm^{-1}. A typical plot to determine the standard deviation is showed in figure 4.12. The overall accuracy of the calibration is therefore 0.1 cm^{-1} or 2×10^{-4} nm.

4.2.3 Optimisation to detect triplet lines

Various experimental parameters were optimised to aid the detection of the lines of forbidden singlet-triplet transitions which will be referred to as triplet lines. The most important of these is the adjustment of the detection gate involving optimisation of both the delay after the laser pulse and the width of the gate i.e. the length of time over which the observed signal is integrated. Other parameters that were optimised was the delay time between the gas pulse

Stellenbosch University http://scholar.sun.ac.za

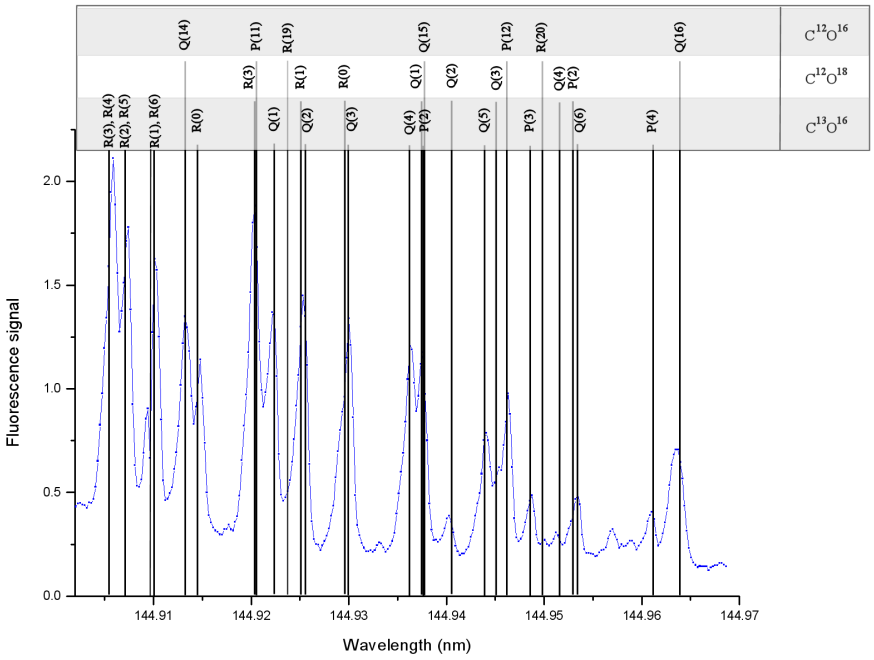

Figure 4.10: A calibrated spectrum of CO showing lines from $^{12}C^{16}O$, $^{13}C^{16}O$ and $^{12}C^{18}O$.

Stellenbosch University http://scholar.sun.ac.za

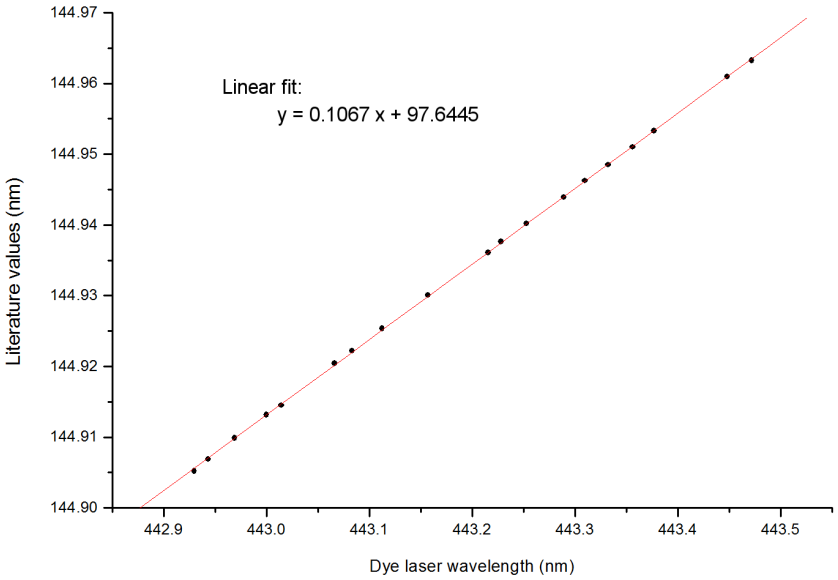

Figure 4.11: An example of a linear fit to a plot of literature wavelengths for CO spectral lines from [3] versus the observed wavelengths of dye laser I. Such a fit has been done for every measured spectrum and was used for wavelengths calibration of the spectrum.

Stellenbosch University http://scholar.sun.ac.za

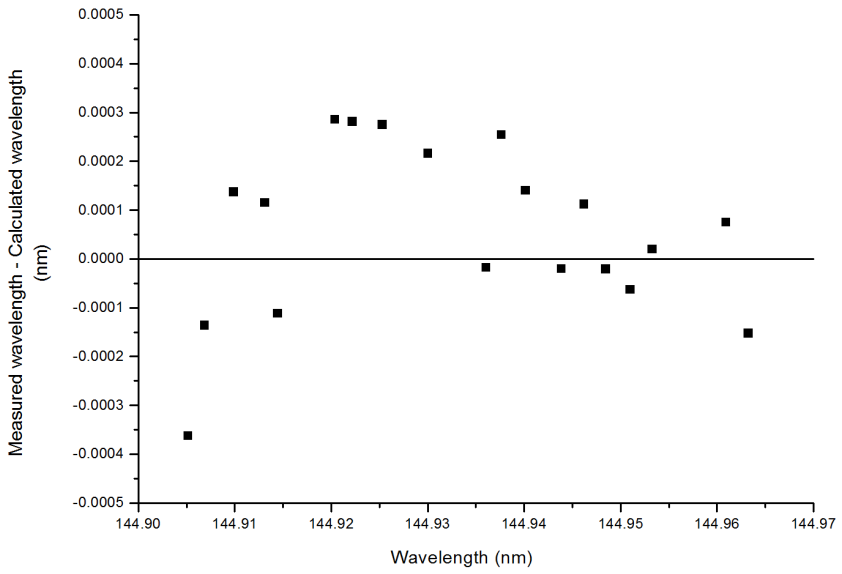

Figure 4.12: An example of the difference between the calibrated wavelengths and literature wavelengths for the lines used in calibration. The standard deviation is typically 1.7×10^{-4} nm.

and the laser pulse as well as the concentration of CO gas in the CO-Ar gas mixture.

4.2.3.1 Detection gate

The effect of the boxcar gate delay and gate width on the signal strength of observed triplet lines were investigated.

The triplet lines that are of interest in this study are weak lines lying in close proximity to strong singlet lines. Generally the singlet states have a much shorter lifetime than the triplet states on account of the higher transition probability between the excited singlet state and the singlet ground state, as opposed to that of the excited triplet state and the singlet ground state. The fluorescence from the singlet-triplet transition therefore decays slower than that of the singlet-singlet transition.

This difference in fluorescence lifetime has been exploited when attempting to observe triplet lines. By increasing the delay of the boxcar gate until the integration gate only starts after the average singlet fluorescence has decayed completely and increasing the width to make best use of the long triplet fluorescence lifetime, the detection of the singlet lines can be suppressed to a certain degree making it possible to observe triplet lines lying in close proximity of them. While this has an adverse effect on the overall signal to noise ratio, it provides a way to observe low intensity triplet lines that would otherwise be obscured by strong singlet lines.

Boxcar gate delays ranging from 30 ns to 200 ns, and boxcar gate widths

Stellenbosch University http://scholar.sun.ac.za

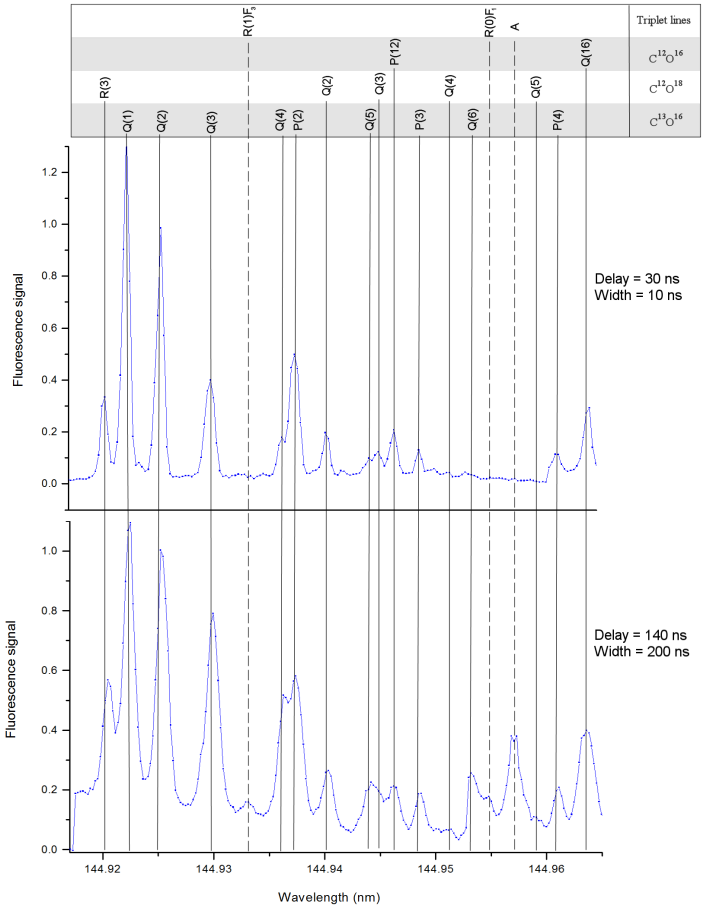

Figure 4.13: A comparison of spectra that were recorded using different boxcar gate width and delay settings.

ranging from 10 ns to 400 ns were investigated. Optimal settings for the observation of triplet lines were found to be a gate delay of $\sim$ 140 ns and a gate width of $\sim$ 300 ns. Figure 4.13 shows a spectrum recorded with gate settings optimised for observation of singlet lines (delay = 30 ns, width = 10 ns) compared to a spectrum recorded with gate settings optimised for observation of triplet lines (delay = 140 ns, width = 200 ns). Three additional lines can be observed in the second spectrum. They have been identified as lines from the $e^3\Sigma^- - X^1\Sigma^+$ band of $^{12}C^{16}O$ as discussed in section 4.2.4. The line labeled A in the figure comprises a group of triplet lines that are not individually distinguishable.

4.2.3.2 Laser and gas pulse timing

Adjusting the delay between the opening of the gas valve and the trigger of the laser pulse changes the position at which the laser pulse passes through the CO gas pulse. Different positions in the gas pulse can differ in terms of temperature

Stellenbosch University http://scholar.sun.ac.za

as well as the density of molecules. The intensity of three triplet lines were observed for three different delay times between the gas pulse and the laser. From the results shown in figure 4.14, it can be seen that the intensity of the triplet lines increases as the delay time is increased. The triplet line intensity also increases relative to singlet line intensity. The optimal setting for delay was found to be around 650 µs. This is very near the end of the gas pulse as a sharp drop in intensity is observed at around 700 µs.

4.2.3.3 Gas mixture

Investigation of the effect of the percentage of CO gas present in the CO - Ar gas mixture was done before other experimental parameters were optimised for observation of triplet lines. For this reason the triplet lines are not visible in the recorded spectra. The optimisation was therefore done by considering the intensity of the singlet lines. It is expected that the conditions in the gas jet that optimises the intensities of the singlet lines should in general also optimise the triplet line intensities with similar values for the J quantum number, although there could be a difference in the optimal setting for strong and weak lines due to self absorption.

Figure 4.15 shows the same section of the spectrum of CO that was recorded for three different concentrations of CO in a mixture of CO and Ar at a total pressure of 4 bars. The signal to noise ratio is relatively low with 0.5 bar of CO in 3.5 bars of Ar, but is observed to increase significantly when the concentration of CO present in the mixture is increased to 1 bar CO in 3 bars of Ar. Another advantage of the increase in CO fraction is that the temperature is higher so that higher J lines can be observed. At 0.5 bar CO only lines with $J \leq 3$ are observable in figure 4.15, whereas higher J lines are observable using the 1 bar CO sample. Increasing the CO concentration further to 3 bars seems to produce a slight drop in the signal to noise ratio of the spectrum. This could be due to less efficient flow cooling of the sample and the effects of self-absorption of the emitted fluorescence in the sample with the higher concentration CO in the mixture. For the purpose of this study the mixture of 1 bar CO in 3 bars of Ar was found to be near optimal and was used for most spectra recorded.

4.2.4 Identification of triplet lines

The wavelengths of the three new spectral lines that were observed in measurements as shown in figure 4.13 do not agree with any singlet lines from any of the four most abundant isotopomers of CO and are therefore likely to originate from triplet transitions. The strongest indicator of the triplet character of the lines is the fact the the measured intensity of the lines increase relative to the intensity of singlet lines as the boxcar gate delay is increased. This points to the longer lifetime associated with the triplet states.

The singlet-triplet vibronic bands from $X^1\Sigma^+(v = 0)$ ground state to the $e^3\Sigma^-(v = 5)$, $d^3\Delta_i(v = 8)$, and $a'^3\Sigma^+(v = 13)$ all have lines that lie in the region of observation. The potential energy curves of each of these excited triplet states overlap the potential energy curve of the $A^1\Pi$ state producing significant spin-orbit perturbations that enhances the transition probabilities for the forbidden singlet-triplet transitions [3]. Transitions from the ground state to the $e^3\Sigma^-(v = 5)$ state have a higher predicted oscillator strength than those

Stellenbosch University http://scholar.sun.ac.za

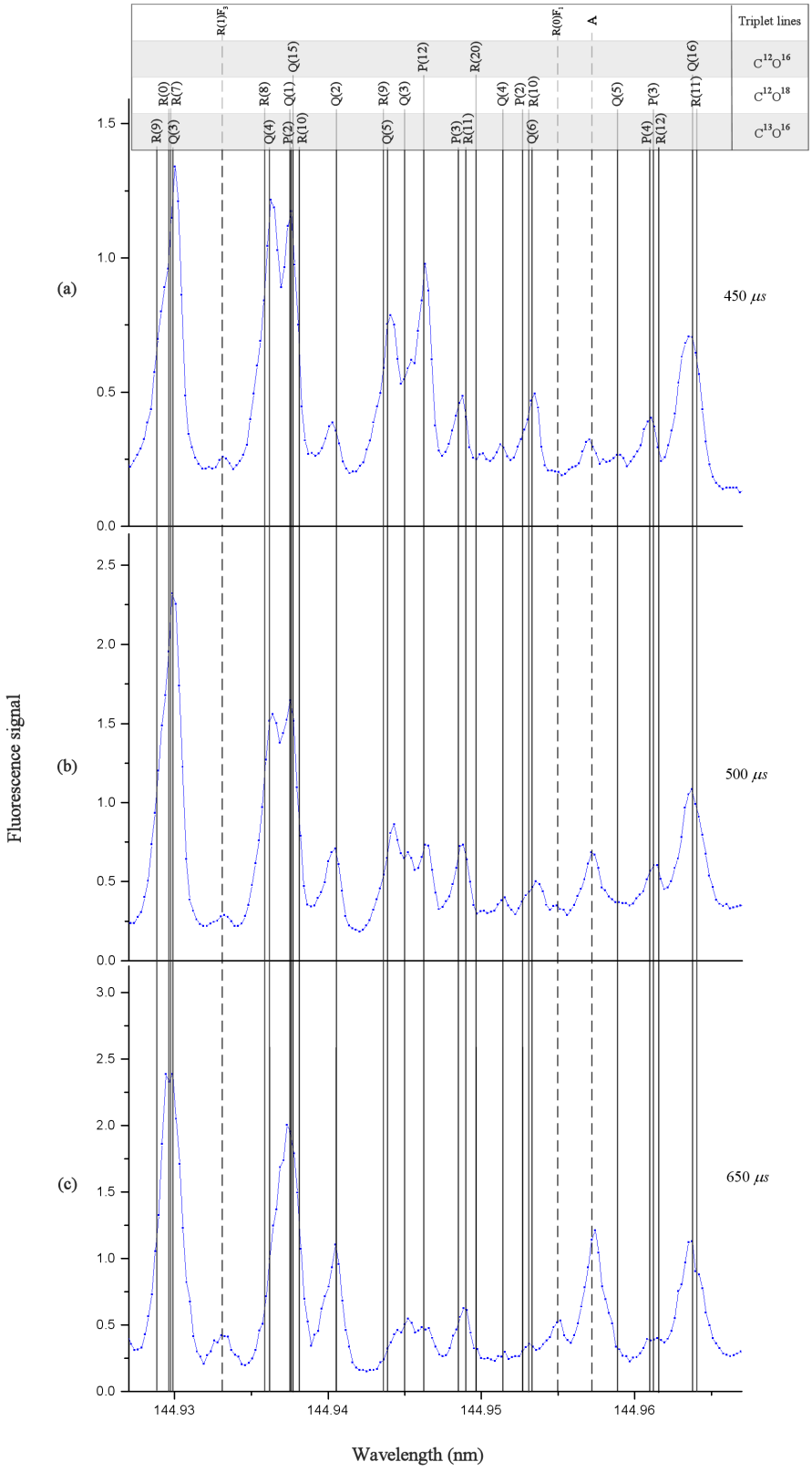

Figure 4.14: A comparison of spectra that were recorded using different delay times between the gas pulse and the laser pulse.

Stellenbosch University http://scholar.sun.ac.za

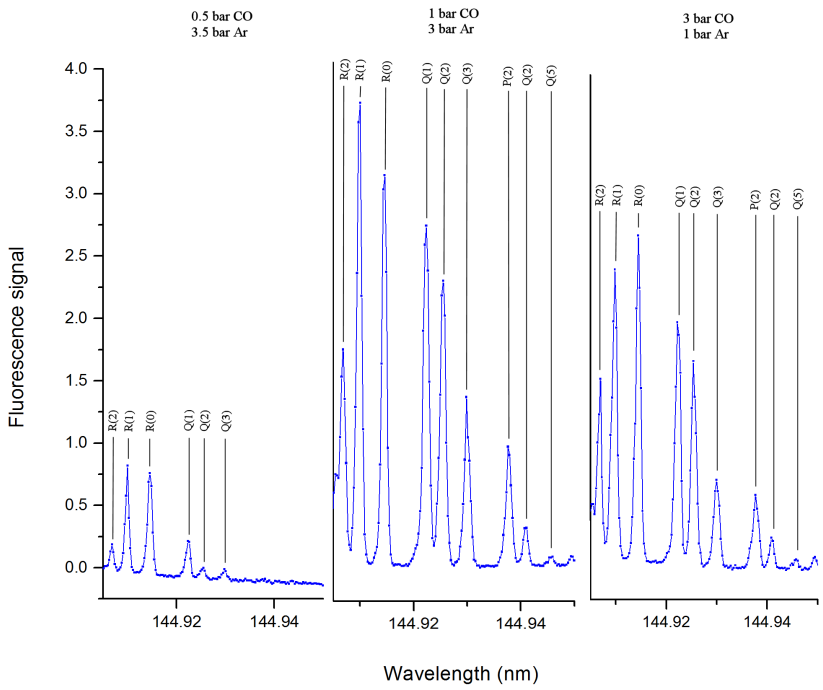

Figure 4.15: A comparison of spectra recorded with different concentrations of CO present in a mixture of CO and Ar at a total pressure of 4 bar

Stellenbosch University http://scholar.sun.ac.za

of the other two states mentioned. Lines from these transitions are therefore expected to be stronger and more readily observed in recorded spectra.

In addition the observed wavelengths of the three new spectral lines correspond well to the wavelengths calculated for lines in the $X^1\Sigma^+(v = 0)$ to $e^3\Sigma^-(v = 5)$ band as published by Eidelsberg and Rostas [4, 19]. These considerations lead to the identification of the three lines as indicated in figures 6.13 and 6.14 to be the following lines in the $X^1\Sigma^+(v = 0)$ to $e^3\Sigma^-(v = 5)$ band: $R(1)F_3$, $R(0)F_1$ and a group of lines (labeled A) that could not be individually resolved comprising of $R(1)F_1$, $Q(1)F_2$ and $R(7)F_3$. Accurate laboratory wavelengths for these lines have not been available previously. The observed wavelengths for these lines along with values for other observed triplet lines that were recorded in subsequent measurements, have been published [20].

Stellenbosch University http://scholar.sun.ac.za

Chapter 5

Summary and Conclusions

5.1 Performance of the VUV laser source using the concentric heat pipe oven

Using the concentric heat pipe oven a nonlinear medium with a length of 30 cm was produced compared to the 6 cm medium previously produced using the crossed heat pipe.

Phase matching curves were recorded under various focusing conditions. For an unfocused beam the spacing between consecutive minima in the phase matching curves were compared for the respective heat pipes. A much smaller average spacing of 0.63 kPa was observed for the concentric heat pipe compared to 3.93 kPa for the crossed heat pipe. This reflects the theoretical dependence of the phase matching factor $F(\Delta kL)$ on the medium length given by equation 2.5 for parallel beams.

By plotting curves through the minima and maxima of a phase matching curve for the concentric heat pipe the modulation depth of the curve was determined to be M = 6.70. From this the optical depth Γ_s was calculated to be 1.63.

When the incoming beam was focused the peak of the phase matching curve was observed to shift in the direction of lower Kr pressure and the modulation depth of the phase matching curve to reduce. The tighter the focusing of the incoming beam the bigger the shift in the peak and the bigger the reduction in modulation depth, showing the gradual transition from the limits of an unfocused beam to a tightly focused beam.

Peak power obtained with the respective heat pipes were compared by observing the maxima of the phase matching curves recorded with an unfocused incoming laser beam. A significant increase in peak power of the produced VUV light was observed when using the concentric heat pipe oven. Measured in arbitrary units a peak power of 2.23 was obtained for the concentric heat pipe and a value of 0.38 for the crossed heat pipe. The ratio of these power values can be rationalised by considering the differences in medium length, magnesium vapour density and beam spot size in the respective measurements.

Stellenbosch University http://scholar.sun.ac.za

5.2 Application to spectroscopy of carbon monoxide

The VUV laser light produced using the crossed heat pipe oven was applied to the spectroscopy of carbon monoxide. Various experimental parameters were investigated and optimal values were found for the observation of CO spectra and in particular the lines of singlet-triplet transitions. The most important parameters for detection of triplet lines are the boxcar gate width and delay times. Optimal values were found to be a gate delay of $\sim$ 140 ns and a gate width of $\sim$ 300 ns.

The delay time between the opening of the gas valve and the firing of the laser pulse was investigated and the optimal value was found to be 650 ms, where the laser pulse will pass through the gas very near the end of the gas pulse.

Finally the concentration of CO gas in the CO-Ar mixture was investigated. The optimal value was found to be 1 bar of CO and 3 bars of Ar.

By applying these optimised conditions we were able to record a number of triplet lines for which accurate laboratory wavelengths have not previously been measured. The results of this study, together with subsequent measurements, were published in the Astrophysical Journal [20].

5.3 Proposed future work

To date only the crossed heat pipe has been incorporated into the experimental setup for the spectroscopy of CO. The increased intensity of VUV light produced with the concentric heat pipe oven should aid the observation of weaker spectral lines. It would be beneficial if the concentric heat pipe could be introduced into this setup in the future.

In order to use the concentric heat pipe to its full potential higher fundamental laser power is required. If the power of the beam is high enough it would remove the need for tight focusing meaning the entire length of the nonlinear medium inside the heat pipe could be utilised.

The region of the spectrum of CO that was investigated during this study is densely populated with many lines overlapping. To be able to resolve overlapping lines and improve the accuracy of line identification a narrower bandwidth VUV laser source is required. This could possibly be obtained by the introduction of an etalon into the tunable dye laser.

Stellenbosch University http://scholar.sun.ac.za

Bibliography

[1] A. Mellinger. *Untersuchung hochangeregter Triplettzustände des CO-Moleküls.* PhD thesis, Technische Universität München und Max Planck Institut für extraterrestrische Physik, 1995.

[2] Hamamatsu. *Data Sheet provided with Hamamatsu R6835.*

[3] D. C Morton and L. Noreau. A compilation of electronic transitions in the CO molecule and the interpretation of some puzzling interstellar absorption features. *The Astrophysical journal supplement series*, 95:301–343, 1994.

[4] M. Eidelsberg and F. Rostas. An atlas of the intersystem transitions of CO. *The Astrophysical Journal Supplement Series*, 145:89–109, 2003.

[5] E.F. Van Drieshoek and J.H. Black. The photodissociation of interstellar CO. *Astrophysical Journal*, 334:771–802, 1988.

[6] C. M. Steinmann. Development and characterisation of a tunable laser source in the vacuum ultraviolet. Master's thesis, University of Stellenbosch, 1999.

[7] Robert W. Boyd. *Nonlinear Optics.* Academic Press, 2003.

[8] C. R. Vidal. *L.F. Molenauer and J.C. White (Eds.), Topics in Appliesd Physics 59*, pages 57–113. Springer Verlag, 1987.

[9] J.F. Ward and G.H.C New. Optical third harmonic generation in gases by a focussed laser beam. *Phys. Rev. 185*, 1:57, 1969.

[10] C. R. Scheingraber, H. & Vidal. Heat pipe oven of well-defined column density. *Review of Scientific Instruments*, 52:1010–1012, 1981.

[11] B. Steffes, X. Li, A. Mellinger, and C. R. Vidal. Heat pipe oven for large column densities with a well-defined optical path lenth. *Appl. Phys. B*, 62:87, 1994.

[12] H. Junginger, H. B. Puell, H. Scheingraber, and C. R. Vidal. Resonant third harmonic generation in a low-loss medium. *IEEE Journal Quantum Electronics*, QE-16, nr. 10:1132, 1980.

[13] R. E. Smalley, L. Wharton, and D. H. Levy. Molecular optical spectroscoy with supersonic beams and jets. *Acc. Chem. Res.*, 10:139–145, 1977.

[14] G. Herzberg. *Spectra of diatomic molecules 1.* Van Nostrand company, New York, 1950. Ed. 2 Fonds Lerch.

Stellenbosch University http://scholar.sun.ac.za

[15] L. M. Beaty, V. D. Braun, and K. P. Huber. A high-resolution 18o isotope study in the vacuum ultraviolet of the a1? - x1?+ 4th positive system of co. *The Astrophysical Journal Supplement Series*, 109:269–277, 1997.

[16] A. du Plessis, E. G. Rohwer, and C. M. Steenkamp. Accurate laboratory wavelengths of the $A^1\Pi(v' = 0 - 5) - X^1\Sigma^+(v'' = 0)$ vibronic bands of $^{12}C^{17}O$ and $^{12}C^{18}O$. *Astrophysical Journal Supplement Series*, 165:432, 2006.

[17] A. du Plessis, E. G. Rohwer, and C. M. Steenkamp. *Journal of Molecular Spectroscopy*, 243:124–133, 2007.

[18] C. M. Steinmann, E. G. Rohwer, and H. Stafast. Accurate laboratory wavelengths of the vacuum ultraviolet $A(v' = 3) - X(v'' = 0)$ band of $^{12}C^{17}O$ and $^{12}C^{18}O$. *Astrophysical Journal*, 590:L123–L126, 2003.

[19] http://amrel.obspm.fr/molat/index.php?page=pages/Molecules/CO-Michele/CO.php.

[20] G. D. Dickenson, A. C. Nortje, C. M. Steenkamp, E. G. Rohwer, and A. du Plessis. Accurate laboratory wavelengths of the $e^3\Sigma^-(v' = 5) - X^1\Sigma^+(v'' = 0)$ band of $^{12}C^{16}O$. *Astrophysical Journal Letters*, 714:L268–L270, 2010.